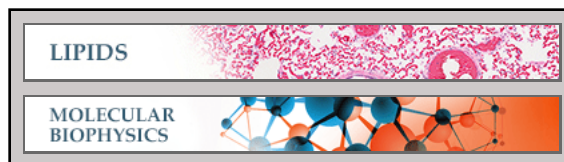Lipids:

Induction of Highly Curved Structures in Relation to Membrane Permeabilization and Budding by the Triterpenoid Saponins, α- and δ-Hederin

LIPIDS

MOLECULAR BIOPHYSICS

Joseph Lorent, Cécile S. Le Duff, Joelle Quetin-Leclercq and Marie-Paule Mingeot-Leclercq

Access the most updated version of this article at doi: 10.1074/jbc.M112.407635

Find articles, minireviews, Reflections and Classics on similar topics on the JBC Affinity Sites.

Alerts:

- When this article is cited
- When a correction for this article is posted

Click here to choose from all of JBC's e-mail alerts

Supplemental material:

http://www.jbc.org/content/suppl/2013/03/25/M112.407635.DC1.html

This article cites 78 references, 9 of which can be accessed free at
http://www.jbc.org/content/288/20/14000.full.html#ref-list-1

Induction of Highly Curved Structures in Relation to Membrane Permeabilization and Budding by the Triterpenoid Saponins, α- and δ-Hederin[S]

Joseph Lorent[‡§], **Cécile S. Le Duff**[¶], **Joelle Quetin-Leclercq**[§], and **Marie-Paule Mingeot-Leclercq**[‡1]

From ‡*Cellular and Molecular Pharmacology and* §*Pharmacognosy, Louvain Drug Research Institute, Université Catholique de Louvain, B-1200 Bruxelles and* ¶*Molecules, Solids and Reactivity, Institute of Condensed Matter and Nanosciences, Université Catholique de Louvain, B-1348 Louvain-la-Neuve, Belgium*

Background: The triterpenoid monodesmosidic saponins, α- and δ-hederin, induced membrane permeabilization.
Results: The membranous cholesterol and the sugars branched on the aglycone, hederagenin, are critical for membrane permeabilization, budding, and the change in lipid phase.
Conclusion: Permeabilization and budding are dependent on the interaction of saponin with cholesterol and the molecular shape of the saponin.
Significance: Induction of curvature by saponins is responsible for permeabilization and budding.

The interactions of triterpenoid monodesmosidic saponins, α-hederin and δ-hederin, with lipid membranes are involved in their permeabilizing effect. Unfortunately, the interactions of these saponins with lipid membranes are largely unknown, as are the roles of cholesterol or the branched sugar moieties (two for α-hederin and one for δ-hederin) on the aglycone backbone, hederagenin. The differences in sugar moieties are responsible for differences in the molecular shape of the saponins and the effects on membrane curvature that should be the most positive for α-hederin in a transbilayer direction. In large unilamellar vesicles and monocyte cells, we showed that membrane permeabilization was dependent on the presence of membrane cholesterol and saponin sugar chains, being largest for α-hederin and smallest for hederagenin. In the presence of cholesterol, α-hederin induced the formation of nonbilayer phases with a higher rate of Brownian tumbling or lateral diffusion. A reduction of Laurdan's generalized polarization in relation to change in order of the polar heads of phospholipids was observed. Using giant unilamellar vesicles, we visualized the formation of wrinkled borders, the decrease in liposome size, budding, and the formation of macroscopic pores. All these processes are highly dependent on the sugars linked to the aglycone, with α-hederin showing a greater ability to induce pore formation and δ-hederin being more efficient in inducing budding. Hederagenin induced intravesicular budding but no pore formation. Based on these results, a curvature-driven permeabilization mechanism dependent on the interaction between saponin and sterols and on the molecular shape of the saponin and its ability to induce local spontaneous curvature is proposed.

Saponins are widely distributed in nature and are known for their physiological, immunological, and pharmacological prop-

erties (1). All of these properties have led to considerable clinical interest in these substances. Currently, however, the mechanisms of action involved in these effects are not completely understood.

Saponins can be classified as either monodesmosidic or bidesmosidic, based on the number of branched sugar chains on the aglycone, as well as into steroid or triterpenoid saponins, depending on the carbon numbers on the aglycone backbone. α-Hederin (also called kalopanaxsaponin A) (2) is a monodesmosidic triterpenoid compound with an α-L-rhamnose-(1→2)-α-L-arabinose sugar chain attached at C3 of the aglycone, hederagenin (Fig. 1). α-hederin was first isolated from the leaves of *Hedera helix* (3). This molecule possesses strong hemolytic activity (4, 5) and cytotoxicity against *in vivo* tumors; in addition, it has *in vitro* effects on various cancer cell lines, which could result from apoptosis (2, 6, 7) and/or membrane alterations (5, 8).

The potential of saponins to interact with biological membranes has drawn much attention. In particular, the interaction with cholesterol has been suggested to be involved in the membrane permeabilization by monodesmosidic saponins with a sugar moiety at C3 (9, 10).

Sterols are essential components of eukaryotic membranes. They enable the cells to modulate the physical properties of membranes in relation to their biological functions (11), including the dynamics and regulation of metabotropic receptors (12). In the mammalian plasma membrane, cholesterol is the most abundant sterol (20–40% mol/mol).

This work aimed to study the interactions of α-hederin and its derivatives that lack one or two sugars (δ-hederin (hederagenin 3-*O*-α-L-arabinopyranoside) and hederagenin) (Fig. 1) with cholesterol and to identify their membrane permeabilizing ability. To understand the molecular mechanism involved and to establish a model explaining their ability to induce membrane permeabilization, we used complementary information afforded by lipid models of mem-

---

α-hederin

δ-hederin

Hederagenin

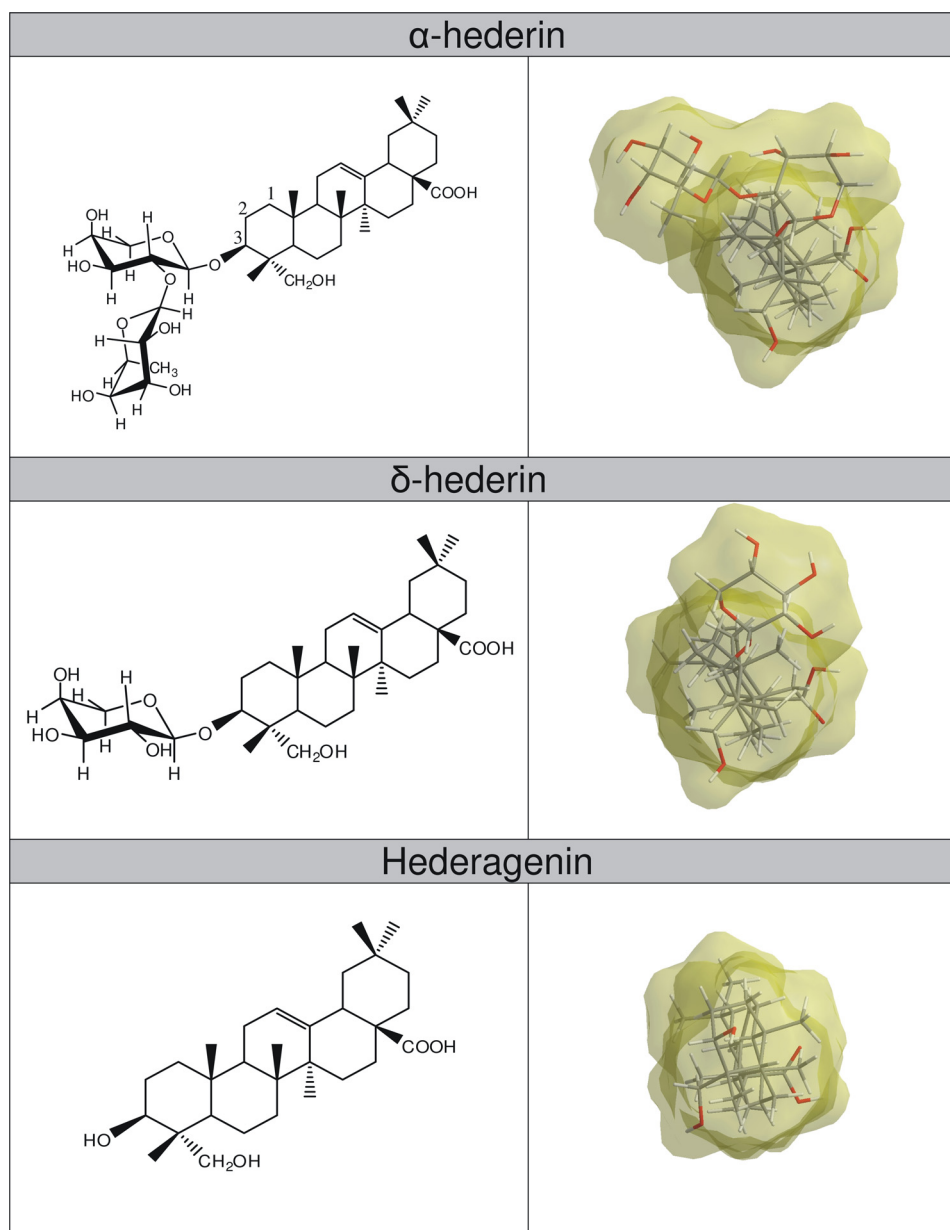FIGURE 1. *Left panels,* two-dimensional chemical structures of α-hederin, δ-hederin, and hederagenin. *Right panels,* three-dimensional structures and molecular shape of minimized energy (view on the C3 residue of the molecule).

branes (large unilamellar vesicles (LUV),[2] multilamellar vesicles (MLV), and giant unilamellar vesicles (GUV)) (13–16). The biological relevance of our study and the importance of membrane cholesterol for cytotoxicity were ascertained by monitoring the effect of α-hederin on a human monocytic cell line depleted or not for cholesterol.

Using LUVs, we measured membrane permeabilization (calcein release), liposome size (dynamic light scattering), and vari-

ations in membrane potential (1-anilinonaphthalene-8-sulfonic acid (ANS)). To obtain further information on the ability of α-hederin to interact with the polar head group region of the membrane, we determined the excitation generalized polarization (GP_{ex}) upon increasing temperature using 6-dodecanoyl-2-dimethylaminonaphthalene (laurdan), which resides at the interfacial region of the bilayer (17–20). The consequences of the interaction of α-hederin with cholesterol on lipid phases were studied by one-dimensional ^{31}P NMR on MLVs.

We took advantage of the size of GUVs to visualize the effects of α-hederin on lipid membrane deformation, budding, and pore formation, and we related these effects to the membrane permeabilization induced by this saponin. To our knowledge, this is the first study investigating the effects of triterpenoid saponins on GUVs.

---

[2] The abbreviations used are: LUV, large unilamellar vesicle; MLV, multilamellar vesicle; GUV, giant unilamellar vesicle; DMPC, phosphatidylinositol 1,2-dimyristoyl-*sn*-glycero-3-phosphocholine; Chol, cholesterol; DHE, dehydroergosterol; TR-DPPE, Texas-Red 1,2-dipalmitoyl-*sn*-glycero-3-phosphoethanolamine; DPH, 6-diphenyl-1,3,5-hexatriene; PI, phosphatidylinositol; PC, phosphatidylcholine; SM, sphingomyelin; ANOVA, analysis of variance; ANS, 1-anilinonaphthalene-8-sulfonic acid.

Membrane Permeabilization and Budding by α- and δ-Hederin

We showed that α-hederin binds to model lipid membranes (LUVs) and to cholesterol, alters the thermotropic behavior of lipids, and forms pores in a cholesterol-dependent fashion. The role of cholesterol and of the branched sugars on the aglycone backbone (α-hederin > δ-hederin > hederagenin) in membrane permeabilization was highlighted. Using GUVs, we visualized potential differences in the permeabilization and deformation of membranes (α-hederin > δ-hederin) or in the production of buds (δ-hederin > α-hederin) in relation to the molecular shape of the saponin and its ability to induce local spontaneous curvature, as we demonstrated using ^{31}P NMR spectroscopy. On a monocyte model, we showed that cell death induced by α-hederin is dependent on the cellular cholesterol content.

This work provides new insights regarding possible molecular mechanisms involved in the pharmacological effects of α-hederin or its derivatives, and this study may renew the clinical interest in saponins, in general.

EXPERIMENTAL PROCEDURES

α-Hederin and hederagenin (HPLC quality) were purchased from Extrasynthèse, (Genay, France). δ-Hederin was kindly provided by Prof. Voutquenne-Nazabadioko (CNRS FRE 2715, IFR 53, Reims, France). The compounds were dissolved in ethanol. After evaporation of the solvent, the residue was resolubilized in a buffer solution (10 mM Tris-HCl adjusted to pH 7.4 with NaOH) in an ultrasonic bath for 1 min. Depending upon the experiments performed, DMSO (maximum 1%) was used for a complete solubilization of α-hederin, δ-hederin, or hederagenin, and the corresponding controls were used. Cells were purchased from ATCC. RPMI 1640 medium was ordered by Invitrogen. Egg phosphatidylcholine, sphingomyelin, phosphatidylinositol 1,2-dimyristoyl-sn-glycero-3-phosphocholine (DMPC), and cholesterol were ordered from Avanti Polar Lipids (Birmingham, AL). The bicinchoninic (BCA) protein assay was purchased from Thermo Scientific. Methyl-β-cyclodextrin (MβCD), calcein, FITC-dextran (4 and 250 kDa), and dehydroergosterol (DHE; Δ5,7,9(11),22-ergostatetraen-3β-ol) were ordered from Sigma. Calcein was purified as described previously (21). 1,8-ANS, 6-dodecanoyl-2-dimethyl-aminonaphthalene (laurdan), Texas-Red 1,2-dipalmitoyl-sn-glycero-3-phosphoethanolamine) (TR-DPPE), and the Amplex® red cholesterol assay kit were purchased from Invitrogen. Polydimethylsiloxane was kindly provided by Henri Burhin and Christian Bailly (Université Catholique de Louvain/Science and Technology Sector/Institute of Condensed Matter and Nanosciences, Louvain-la-Neuve, Belgium). All other reagents were purchased from Merck.

Molecular Modeling of α-Hederin, δ-Hederin, and Hederagenin—Molecules were drawn in ChemDraw Ultra 10.0 and then visualized in three-dimensions by Chem three-dimensional Ultra 10.0. A minimized energy structure was calculated, and the molecular surface shape displayed using the "Connolly molecular" mode.

Incubation with α-Hederin of THP-1 Monocytes Depleted or Not in Cholesterol—Cells were cultivated in RMPI 1640 medium supplemented with 10% fetal calf serum in 95% air and 5% CO_2.

For cholesterol depletion, cells (10^6 cells/ml) were harvested and incubated for 2.5 h in fresh RPMI 1640 medium supplemented with 1 mg/ml BSA and 5 mM methyl-β-cyclodextrin (MβCD) (22). Cell counting was performed in a Burker chamber. After this incubation, cells were washed three times with RPMI 1640 medium. At this time, part of the cells was quantified for the cholesterol and protein content with the Amplex® Red cholesterol assay and BCA protein assay kit, respectively. The other part was incubated with increasing concentrations of α-hederin. Cell death was quantified by the trypan blue assay and given in percent of total cells.

Preparation of MLVs and LUVs—DMPC or DMPC/Chol (3:1) MLVs were prepared according to the freeze-thawing method as described previously (23) in a buffer solution (10 mM Tris-HCl, pH 7.4).

LUVs composed of PC/SM/PI/Chol (4:4:3:0, 4:4:3:2.25, or 4:4:3:5.5), DMPC, or DMPC/Chol (3:1) were prepared by the extrusion technique (24), using a 10-ml Thermobarrel extruder (Lipex Biomembranes, Vancouver, Canada). The MLVs were extruded at 45 °C, 10 times through two superimposed track-etch polycarbonate membranes (pore size = 100 nm; Whatman Nucleopore, Corning Costar Corp., Badhoevedorp, The Netherlands) to obtain LUVs. The lipid concentration of the liposomal suspension was measured by phosphorous quantification (25) and adjusted according to the experimental protocol used.

Release of Calcein Entrapped at Self-quenching Concentration within LUVs—The leakage of entrapped self-quenched calcein from LUVs induced by a permeabilizing agent can be monitored by the fluorescence increase caused by its dilution (26).

For these permeability studies, the lipid film was resuspended in a purified calcein solution (72 mM calcein and 10 mM Tris-HCl) adjusted to pH 7.4 and 400 mosm/liter (measured by the freezing point technique (Knauer osmometer automatic, Berlin, Germany)). The unencapsulated calcein was removed using the minicolumn centrifugation technique (27).

The calcein-filled liposomes (5 μM lipids) were incubated with α-hederin at 37 °C for increasing periods of time. The percentage of calcein released was determined as described previously (28). The excitation and emission wavelengths were 472 and 512 nm, respectively. All steady-state fluorescence experiments were performed on an LS55 luminescence spectrometer (PerkinElmer Life Sciences).

DHE Steady-state Spectroscopy—The ability of α-hederin to bind to cholesterol was investigated using DHE fluorescence spectroscopy. DHE is a structurally close cholesterol analog presenting a similar behavior in aqueous solution and biological membranes as cholesterol (29–31).

When DHE is excited at 310 nm in aqueous solution, it presents a low intensity monomeric peak at 375 nm and a high intensity maximum of structured emission at 395 and 424 nm due to the presence of microcrystals in buffer solution. Therefore, the ratio between fluorescence intensities at 375 *versus* 395 or 424 nm (I_{375}/I_{395} or I_{375}/I_{424}) reflects the ratio of monomers *versus* microcrystals in aqueous solution. Moreover, a decrease in the dielectric constant of the microenvironment of DHE induces a blue shift of λ_{max} emission (29).

DHE was solubilized at 4 μg/ml in buffer solution containing 0.1% DMSO. Increasing α-hederin concentrations were added. The emission spectrum was taken at excitation wavelength of 310 nm. To confirm formation of aggregates composed of α-hederin and cholesterol, we incubated both compounds at equimolar concentration (500 μM) in buffer solution at 1% DMSO and looked for the formation of a macroscopic precipitate.

DHE was also incorporated in MLVs composed of DMPC/Chol/DHE (75:24:1) to probe the effect of α-hederin on cholesterol in a lipid environment. Maximal emission of DHE was observed around 355, 375, and 390 nm, as described previously in membrane systems. Seras *et al.* (32) observed no spectral shift during the transformation of bilayers into micelles but reported a decrease in fluorescence lifetime and intensity. The MLVs were incubated for 3 h at 25 °C at increasing α-hederin/total lipid ratios.

Dynamic Light Scattering and ANS Fluorescence—The apparent average diameter of LUVs was determined by dynamic light scattering spectroscopy using a Malvern Zetasizer Nano ZS® (Malvern Instruments, Ltd., Worcestershire, UK). The fluctuation of light scattering was measured at an angle of 90° with monodisperse latex particles with diameters of 100 and 800 nm as controls. The data were collected using the size distribution analysis mode to determine the full size distribution profile of the liposomes incubated with α-hederin. The membrane potential differential was assessed with ANS, a probe that fluoresces when it is bound to lipid membranes (33, 34) and characterized by its sensitivity to superficial charges on the membrane surface. An ANS stock solution of 5 mM in methanol was prepared. The fraction of ANS bound to the membrane and the variation of surface potential of the liposomes caused by α-hederin were determined as described previously (35).

One-dimensional ^{31}P NMR Spectroscopy on MLVs—MLVs (30 mg of total lipid in Tris-HCl, pH 7.4) were prepared according to the freeze-thaw method. Because ^{31}P NMR spectroscopy requires high amounts of products, we avoided the solubility problem by inserting compounds during the formation of the lipid film. As a positive control, we used SDS, which is known to be cone shaped and to induce positive curvature (36).

0.3 ml of D_2O was added for deuterium lock to 2.5 ml of sample. This sample was placed in a 10-mm Wilmad 513-pp NMR tube that rotated at 20 rpm in the NMR spectrometer.

NMR spectra were acquired on a Bruker Avance DRX500 spectrometer operating at 500.13 MHz for ^1H (202.47 MHz for ^{31}P) and equipped with a 10-mm Bruker broad band observe probe.

The temperature in the probe was regulated at 37 or 60 °C for the duration of the experiments. All ^{31}P spectra were referenced to the ^{31}P peak from an 85% solution of phosphoric acid (H_3PO_4) measured at 25 °C (set at 0 ppm).

One-dimensional ^1H spectra were recorded prior to ^{31}P experiments to ensure the best field homogeneity was attained for each sample. 114,688 points and an acquisition time of 0.7 s using power-gated Waltz16 ^1H decoupling were used, and 26,000 scans per ^{31}P experiment with a sweep width of 83.1 kHz were acquired with a delay of 1.5 s between scans. The signal was Fourier-transformed using an exponential multiplication

function with a line broadening of 50 Hz and zero-filled to a final spectral resolution of 0.6 Hz per point.

Laurdan Generalized Polarization—Using LUVs, the effect of the drugs on the mobility of phospholipids and the polarity at the level of the glycerol backbone were determined by monitoring the Laurdan excitation generalized polarization (GP_{ex}) (17, 37). Upon excitation, the dipole moment of laurdan increases noticeably, and water molecules in the vicinity of the probe reorient around this new dipole. When the membrane is in a fluid phase, the reorientation rate is faster than the emission process, and consequently, a red-shift is observed in the emission spectrum of laurdan. When the bilayer packing increases, some of the water molecules are excluded from the bilayer, and the dipolar relaxation rate of the remaining water molecules is slower, leading to an emission spectrum that is significantly less red-shifted. The GP_{ex} allows quantification of this red-shift from the emission spectra.

The lipid concentration of the liposome solution was adjusted to 25 or 50 μM with 10 mM Tris-HCl at a pH of 7.4. Laurdan (5×10^{-3} M stock solution in tetrahydrofuran) was added to the lipid film to obtain a lipid/probe ratio of 300. Then α-hederin or hederagenin was added to the liposomes at a final concentration of 30 or 60 μM and incubated under continuous agitation at 37 °C in the dark for 60 min. The generalized polarization values from the emission spectra were calculated using Equation 1,

$$GP_{ex} = \frac{I_{440} - I_{490}}{I_{440} + I_{490}}$$

(Eq. 1)

where I_{440} and I_{490} are the fluorescence intensities at emission wavelengths of 440 nm (gel phase) and 490 nm (liquid crystalline phase), respectively, at a fixed excitation wavelength of 340 nm. The generalized polarization was determined as a function of temperature.

Depending on the shape of the curves, the best adjustment was selected. For DMPC/Chol and DMPC, GP_{ex} values as a function of temperature were adjusted using the Hill equation or a five-parameter Richards function, respectively (38).

Preparation of GUVs—GUVs were prepared by electroformation (39). Briefly, 1 μl of a chloroform solution of DMPC/Chol (3:1; 5 mg/ml), was spread on an indium tin oxide-covered glass. The fluorescent probes were added to the chloroform solution at a concentration of 0.1% mol/mol. The solution was dried in a vacuum chamber for 2 h. An electroformation chamber was constructed using another indium tin oxide-covered glass slide, with the conducting face pointed toward the interior of the electroformation chamber, which was filled with a 0.1 M saccharose solution. Polydimethylsiloxane containing 5% fumed silica was used to separate the two glass slides. The GUVs were grown by applying a sinusoidal alternating current of 10 Hz and 1 V for 2 h at 60 °C.

Fluorescence and Confocal Microscopy of GUVs—The GUVs were labeled with TR-DPPE (40), which was excited at 561 nm and recorded at 617 nm. In the fluorescence microscopy experiments, we used an Axioskop 40 microscope (Carl Zeiss, Jena, Germany) with a 40×/0.75 Zeiss EC Plan-Neofluar® objective,

and the images were recorded with a Nikon digital sight DS-5 M camera (Nikon, Tokyo, Japan).

For the confocal microscopy experiments, an Axio-observer spinning disk inverted microscope Z.1 (Carl Zeiss, Jena, Germany) was utilized. The spinning disk was a CSU-X1 model (Yokogawa Electric Corp., Tokyo, Japan). The objectives used included an LD LCI Plan-Apochromat 25×/0.8 Imm Korr DIC M27, an EC Plan-Neofluar 40×/1.30 Oil DIC M27, an LCI Plan-Neofluar 63×/1.30 Imm Korr DIC M27, and a Plan-Apochromat 100×/1.40 Oil DIC M27. The images were recorded with an AxioCamMR3 camera using the Carl Zeiss AxioVision 4.8.2 software.

Permeability of Dextran through Membranes of GUVs—After electroformation, 10 μl of GUVs were added to a solution containing 20 μM FITC-dextran (mean molecular weight of 4 or 250 kDa) and 40 μM α-hederin, δ-hederin, or hederagenin. As positive control, we used 30 mM SDS. The FITC-dextran was excited at 488 nm, and the emission was recorded with a 520/35-nm emission filter and visualized as described previously (41). We chose GUVs that presented typical deformation features and followed one GUV with fluorescence microscopy at corresponding time points. The difference in fluorescence intensity between the outside and inside of one GUV reflects the membrane integrity. In contrast, similar fluorescence intensities indicate the penetration of the fluorescent probe. The difference in fluorescence intensity outside and inside the vesicle was calculated by dividing the fluorescence values by the highest intensity recorded and multiplying by a factor of 1000. The difference of the mean of 20 normalized values taken from inside and outside the vesicle was then determined. The significant difference was calculated using a Student's *t* test.

Deformation, Pore Formation, and Budding of GUVs—After electroformation, 30 μl of the GUVs were added to a saccharose solution (0.1 M; DMSO 0.1%) containing 40 μM α-hederin, δ-hederin, or hederagenin. As positive control, we used 400 μM, 4 mM, and 30 mM SDS. The deformation of the vesicles was followed for at least 50 min (except for 30 mM SDS where complete dissolution occurred after several minutes). An initial image was captured immediately after the vesicles were added to the solution containing one of the three compounds. Subsequent images were taken at regular intervals thereafter. Because photobleaching reduced the visibility of the vesicle, the luminosity and contrast were enhanced by the acquisition software (NIS-Elements D 3.10, Nikon, Tokyo, Japan). Selected images were used to visualize by fluorescence and confocal microscopy the pore formation and budding of vesicles upon increasing times of exposure. In the confocal microscopy experiments, we chose a cross-section that passed through the middle of the vesicle. Three-dimensional images represented the superimposition of all of the cross-sections obtained from one vesicle. The quantification of vesicles presenting different features (wrinkled membrane deformation, pore formation, budding, or aggregation) was achieved by counting a total of 200 vesicles after 0.5 or 1 h of incubation with the compounds.

Statistical Analysis—All statistical analyses were performed using GraphPad Prism version 4.00 for Windows (GraphPad Software, San Diego) with a two-way ANOVA using all data points to compare plots or a Student's test when dextran fluo-
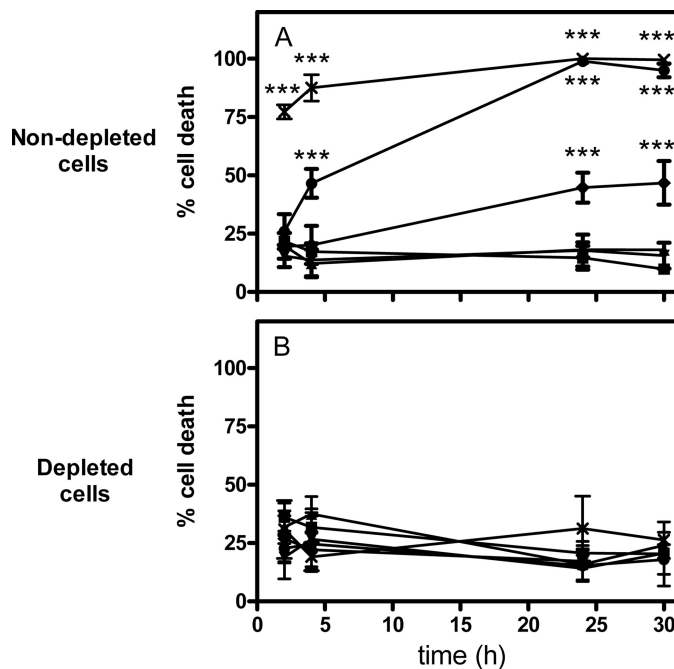

FIGURE 2. **Trypan blue assay of nondepleted and cholesterol-depleted THP-1 cells incubated for 2, 4, 24, and 30 h with increasing α-hederin concentrations.** Control (■), 10 (▲), 15 (▼), 20 (♦), 25 (●), and 30 μM (×). Each value is the mean of four independent assays ± S.D. Statistical analysis: two-way ANOVA comparing each data point for normal *versus* depleted cells. ***, $p < 0.001$.

rescence intensities inside and outside the vesicles were compared. For the nonlinear regression of laurdan GP_{ex} in the DMPC LUVs, we used a five-parameter Richard's function in JMP 8.01.

RESULTS

Cell Death Induced by α-Hederin in Cells Depleted or Not in Cholesterol—Using trypan blue assay, we investigated the cytotoxicity of α-hederin on a human leukemic monocytic cell line (THP-1) and the role of membrane cholesterol (Fig. 2). Cell membranes were depleted in cholesterol by MβCD (22), and cholesterol content was quantified after incubation. Nondepleted THP-1 cells had a free cholesterol amount of 12.55 ± 0.68 μg of cholesterol/mg of protein whereby depleted cells showed 6.80 ± 1.17 μg/mg. We can assume that this depletion is mainly due to the depletion of the plasma membrane because 90% of the total cholesterol content of the cell is found in the plasma membrane (42). Results show that on nondepleted cells, the cytotoxicity induced by α-hederin in THP-1 was concentration- and time-dependent (Fig. 2*A*). In contrast, when cells were depleted in cholesterol, almost any cytotoxicity was observed (Fig. 2*B*). Hederagenin at 30 μM did not significantly increase cell death for at least 24 h of incubation regardless of the cholesterol content (data not shown).

Membrane Permeabilization Induced by α-Hederin, δ-Hederin, and Hederagenin on LUVs and GUVs—To investigate the effect of α-hederin and its derivatives on lipid membrane permeability, we determined the ability of α-hederin, δ-hederin, and hederagenin to induce release of calcein from LUVs and permeation of dextran of 4 and 250 kDa through GUV mem-
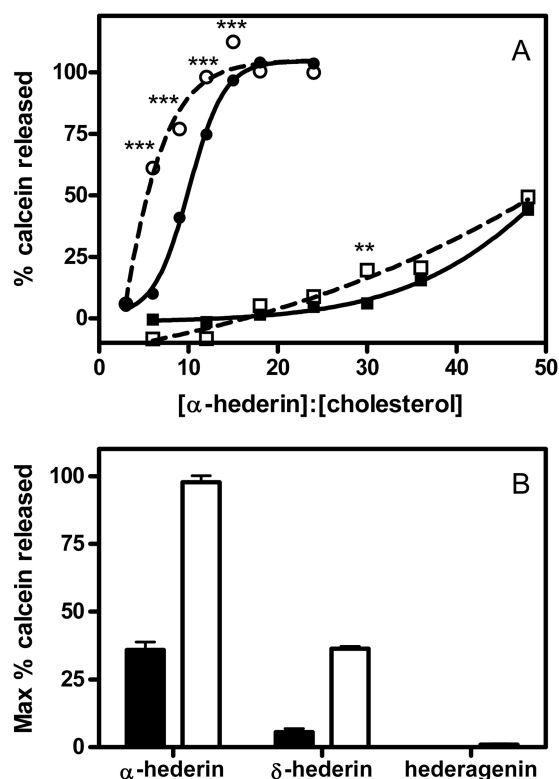
FIGURE 3. *A*, release of calcein from liposomes (5 μM of total lipids) upon exposure at 37 °C for 30 min (*solid lines; filled symbols*) or 18 h (*dashed lines; open symbols*), upon increasing α-hederin/cholesterol ratios. The liposomes were made of PC/SM/PI/Chol (4:4:3:5.5) (*circles*), PC/SM/PI/Chol (4:4:3:2.25) (*squares*). The *graph* shows the functions obtained by fitting a one-phase exponential association function to the data by nonlinear regression. *B*, maximal release of calcein from liposomes composed of DMPC/Chol (3:1) upon exposure at 37 °C to α-hederin, δ-hederin, or hederagenin at a compound/cholesterol molar ratio of 16 (*closed histogram*) or 48 (*open histogram*). Because of the partial insolubility of α-hederin, δ-hederin, and hederagenin, the three compounds were dissolved in DMSO (final solution 0.5% DMSO). The *ordinate* shows the percentage of calcein released compared with what was observed after addition of 2% Triton X-100. Each value is the mean of triplicate ± S.D. (when not visible, the *bars* are smaller than the symbols). Statistical analysis: two-way ANOVA comparing each data point for 30-min and 18-h incubations: **, $p < 0.01$; ***, $p < 0.001$.

branes. Using LUVs, we also questioned the roles of cholesterol for membrane permeabilization induced by α-hederin.

We first used LUVs containing PC/SM/PI/Chol, a lipid mixture mimicking the lipid composition of the plasma membranes (43), to characterize the effect of α-hederin and hederagenin on membrane permeability. To investigate the importance of cholesterol, we prepared liposomes with varying contents of cholesterol (PC/SM/PI/Chol, 4:4:3:0, 4:4:3:2.25, or 4:4:3:5.5). With increasing cholesterol content (from 0 to 33.3%), α-hederin induced a greater release of calcein, even at an equal α-hederin/cholesterol ratio (Fig. 3A). In the absence of cholesterol, no release of calcein was observed (data not shown). At the highest cholesterol composition (PC/SM/PI/Chol, 4:4:3:5.5) and after 18 h of incubation, the release of calcein reached more than 50% at an α-hederin/cholesterol ratio of 6 and reached 100% at a ratio of 12 (Fig. 3A). Under these conditions, the duration of incubation was also a critical parameter because the release of calcein increased with the time of incubation (18 h *versus* 30 min) (Fig. 3A). Upon addition of hederagenin, no release of

calcein was observed regardless of the cholesterol content, the time, or the hederagenin/lipid molar ratio (data not shown).

The role of the branched carbohydrate chain on hederagenin in membrane permeabilization was confirmed using binary liposomes composed of DMPC/Chol (3:1) (Fig. 3B). At both compound/cholesterol ratios of 16 and 48, there is a clear relationship between the number of sugars and the release of calcein, with α-hederin inducing the greatest release, followed by δ-hederin and hederagenin.

To decipher the mechanism involved, we also performed permeabilization experiments using GUVs. We therefore visualized by confocal microscopy the evolution of the concentration profile of FITC-dextran (Fig. 4) at molecular masses of 4 kDa (Fig. 4, *A, C,* and *E*) and 250 kDa (Fig. 4, *B* and *D*) outside and inside the vesicle. We followed the effect induced by α-hederin (Fig. 4, *A* and *B*), δ-hederin (Fig. 4, *C* and *D*), and hederagenin (Fig. 4E) at corresponding stages of membrane deformation. The control images were obtained by adding GUVs to an equimolar sucrose solution containing FITC-dextran.

In the control solutions, FITC-dextran was located outside the vesicle, and a large difference in fluorescence intensities between the outside and inside of the GUVs was observed for the whole duration of the incubation. Upon addition of GUVs to the α-hederin solution, the difference between FITC-dextran (4 kDa) concentration located outside and inside was quickly suppressed as a result of the penetration of FITC-dextran through α-hederin-induced pores in the lipid membrane (Fig. 4A). The permeabilization was observed before any deformation of the vesicle was visible. A permeabilization was also observed with the higher molecular weight FITC-dextran (250 kDa), but the rate was slower (Fig. 4B).

Regarding the effect of δ-hederin when FITC-dextran 4 kDa was used, we also observed a decrease in the difference in fluorescence intensities outside and inside the vesicle, but which appeared later as observed with α-hederin (Fig. 4C). When FITC-dextran of 250 kDa was used, almost no effect was observed after over 2 h of incubation for δ-hederin (Fig. 4D).

Our results suggested that both α-hederin and δ-hederin have the ability to induce a time-dependent growth of pore size, with α-hederin being more efficient. In contrast, hederagenin was unable to induce permeation of FITC-dextran (4 kDa) even after 24 h of incubation (Fig. 4E).

SDS, a cone-shaped detergent, was used as a positive control. It induced a fast suppression of the dextran gradients at 30 mM (supplemental Fig. S1). Micrometer sized pores appeared nearly simultaneous to the permeabilization (supplemental Fig. S2, pores).

All these results suggest that membrane permeabilization induced by α-hederin was increased by the following: (i) the cholesterol content of the liposomes; (ii) the time of incubation; (iii) the α-hederin/cholesterol ratio, and (iv) the number of sugars attached to the C3 residue. Pore size seemed to increase with time. Moreover, permeation to a low size dextran (4 kDa) was faster than to the large size dextran (250 kDa) and was higher for α-hederin when compared with δ-hederin.

Binding of α-Hederin to Sterols and Membranes—Because cholesterol plays a critical role in membrane permeabilization induced by α-hederin, we explored the ability of the latter to
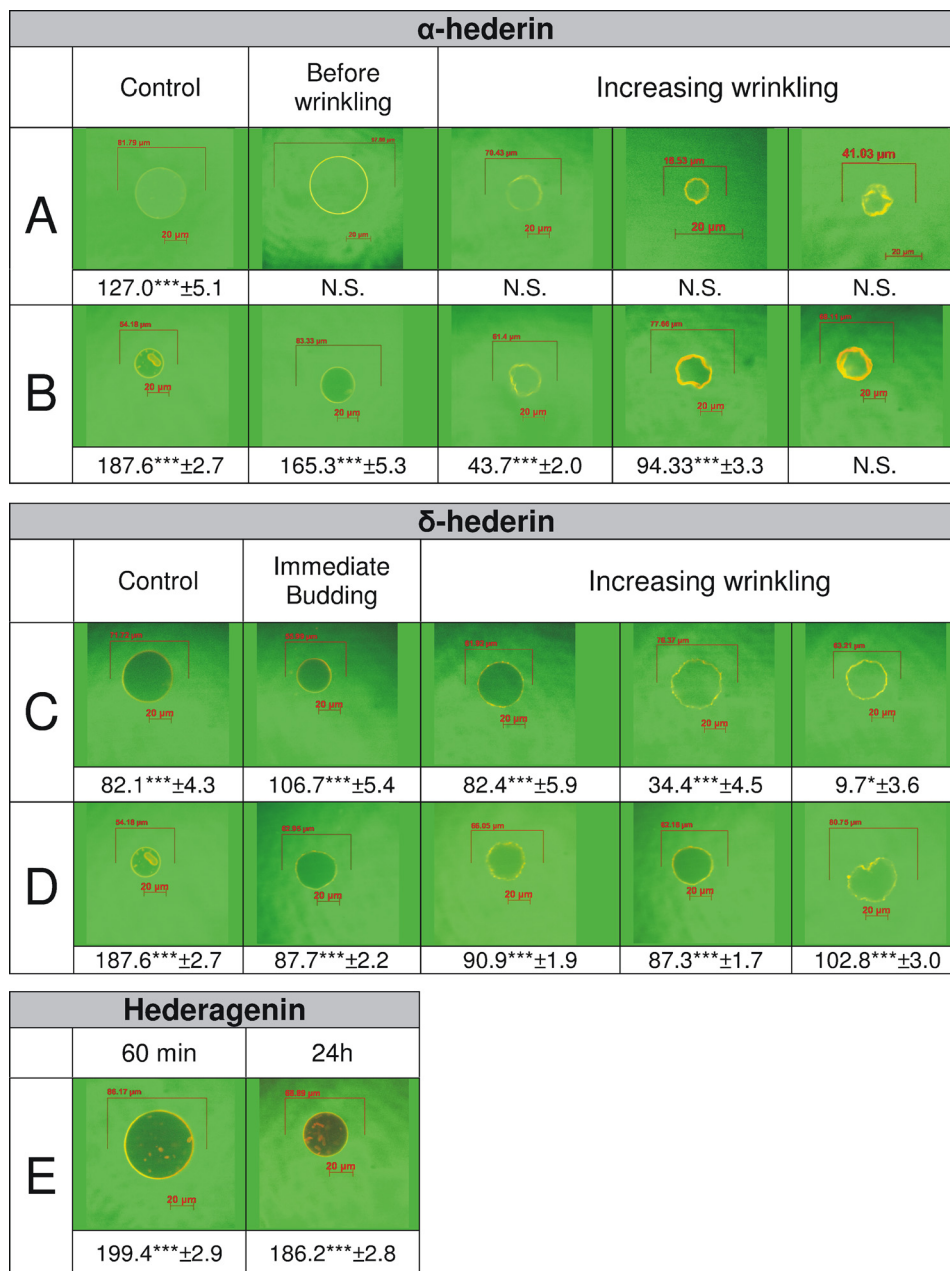
FIGURE 4. **Effect of α-hederin, δ-hederin, or hederagenin on the permeability to FITC-dextran 4 kDa (*A*, *C*, and *E*) or 250 kDa (*B* and *D*) of GUVs composed of DMPC/Chol (3:1) and labeled with TR-DPPE, at different stages of deformation.** For each stage, the difference of normalized fluorescence between inside and outside of the vesicle was quantified. For hederagenin, no deformation was observed. Statistical analysis (*t* test): ***, $p < 0.001$. *N.S.* means no significant difference.

bind to dehydroergosterol (DHE), a fluorescent analog of cholesterol (29–32), or to change membrane surface potential of DMPC/cholesterol vesicles as compared with DMPC liposomes. To address these questions, we used fluorescence spectroscopy of DHE and ANS, respectively.

In an aqueous environment, and upon increasing α-hederin/DHE ratios, we observed a global increase of fluorescence intensities and specifically an increase of the intensity ratio (I_{375}/I_{395}) (Fig. 5A). This ratio reached 0.63 ± 0.05 in control solution and 0.90 ± 0.03 with a α-hederin/DHE molar ratio set at 4. Moreover, the maximum of the structured emission was undergoing a blue shift from 424 to 419 nm, reflecting a more hydrophobic environment for DHE (29, 31). Both results indi-

cate the formation of dehydroergosterol/α-hederin micelles or aggregates, which clearly points out the affinity of α-hederin for DHE. The formation of macroscopic aggregates was observed when α-hederin and cholesterol were co-incubated at equimolar concentrations (500 μM).

In MLVs, upon increasing concentrations of α-hederin, we observed an important decrease of DHE fluorescence intensity after 3 h of incubation (Fig. 5B). In contrast, the intensity ratio did not change significantly, and we observed no shift of the maxima. The same behavior of DHE was observed with octyl glycoside (32) and could be related, as suggested by the authors, to a reduction of fluorescence lifetime of DHE in mixed micellar lipid aggregates. Therefore, the results
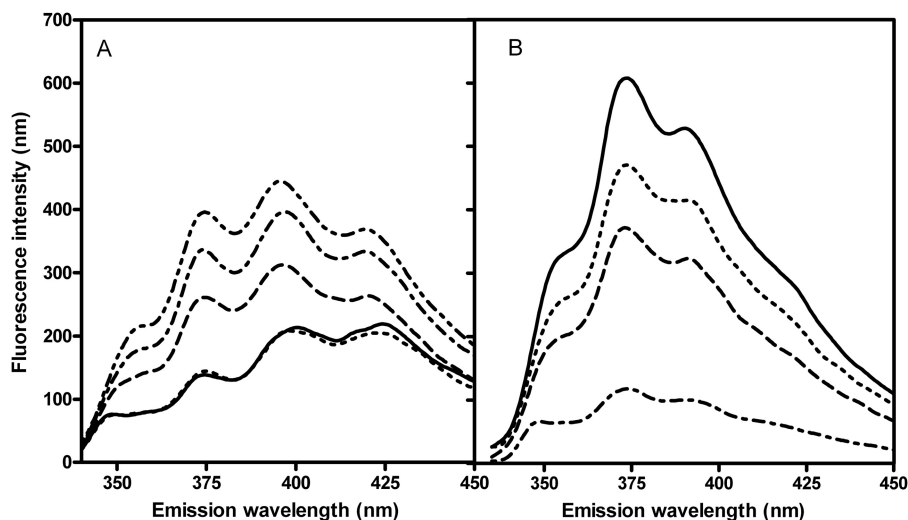
FIGURE 5. **Fluorescence emission spectra of DHE (*A*) in aqueous solution (4 μg/ml and 0.1% DMSO) and MLV (*B*) composed of DMPC/Chol/DHE (75:24:1).** Excitation wavelength was set at 310 nm. In aqueous solution, spectra were recorded upon increasing α-hederin/DHE ratios. Control (*solid line*), 0.5 (*dotted line*), 1.5 (*dashed line*), 2 (*dash dot line*), and 4 (*dash dot dot line*). In MLV after incubation for 3 h (25 °C) at increasing α-hederin/total lipids ratios, spectra were taken. Control (*solid line*), 0.1 (*dotted line*), 0.3 (*dashed line*), and 0.6 (*dash dot line*).

TABLE 1

Variation of membrane surface potential ($\Delta\psi$ and corresponding intervals of confidence) of LUVs incubated with α-hederin or hederagenin

Compound/ lipid ratio	10 min, α-hederin		60 min			
			α-Hederin		Hederagenin	
	DMPC	DMPC/Chol	DMPC	DMPC/Chol	DMPC	DMPC/Chol
1.2	−1.89 (−5.33; 1.70)	−1.43 (−5.39; −2.72)	−14.75 (−17.53; −12.01)	+0.53 (−7.09; 7.28)	−5.09 (−9.58; −0.97)	−6.00 (−9.81; −2.15)
2.4	−14.78 (−21.74; −8.63)	−11.41 (−16.04; −6.66)	−16.09 (−19.31; −12.99)	−3.27 (−7.00; 0.31)	−8.56 (−11.16; −5.99)	−9.29 (−16.06; −3.42)

strongly suggest that α-hederin induces nonbilayer mixed lipid aggregates.

Second, the critical role of cholesterol for binding of α-hederin to liposomes was ascertained by determining the $\Delta\Psi$ of liposomes (Table 1) of DMPC or DMPC/Chol (3:1) upon increasing incubation times and α-hederin/lipid molar ratios. After an incubation time of 10 min, with α-hederin/lipid ratios of 1.2 and 2.4, $\Delta\Psi$ decreased in DMPC and DMPC/Chol liposomes. When the liposomes were incubated with α-hederin for 1 h, the surface potential of the DMPC liposomes reached more negative values, whereas $\Delta\Psi$ showed slightly positive or negative values when α-hederin was incubated with DMPC/Chol (3:1) liposomes. In contrast, upon addition of hederagenin, the decrease in $\Delta\Psi$ was similar for liposomes with or without cholesterol after 60 min of incubation.

At a glance, cholesterol was probably critical for the interaction of α-hederin with lipid membranes as suggested by the change in fluorescent properties of DHE and the formation of a precipitate when α-hederin and cholesterol were co-incubated in aqueous solution. In a bilayer environment, α-hederin interacts with DHE (and most probably with cholesterol) and forces it into mixed nonbilayer lipid aggregates.

The reduction of membrane surface potential of liposomes incubated with α-hederin suggests that the saponin binds independently of the presence of cholesterol to the membrane. However, at longer incubation periods, the presence of cholesterol reversed the decrease of the surface potential, indicating its important role for membrane interaction.

Changes in Liposome Size and Appearance of New Structures Induced by α-Hederin—To decipher if the interaction between α-hederin and cholesterol results in variations of liposome size and changes in lipid organization, we determined the size of DMPC and DMPC/Chol LUVs upon increasing α-hederin/ cholesterol ratios, using dynamic light scattering. We also characterized the phospholipid organization in MLVs where α-hederin had been integrated within the lipid film, using one-dimensional ^{31}P NMR spectroscopy.

First, we showed the effect of α-hederin on the size of LUVs composed of DMPC (Fig. 6, *A* and *B*) or DMPC/cholesterol (3:1 molar ratio; Fig. 6, *C* and *D*) after 1 h (Fig. 6, *A* and *C*) and 24 h (Fig. 6, *B* and *D*) of incubation at 37 °C with increasing amounts of α-hederin. In the absence of cholesterol, regardless of the duration of incubation or the concentration of saponin, no change in the mean size of the liposomes was observed (Fig. 6, *A* and *B*). This lack of effect was in strict contrast to what was observed when the liposomes contained cholesterol. In such samples, two main populations of liposomes emerged (Fig. 6, *C* and *D*). One was centered at smaller sizes and the other at higher sizes than the original (100 nm). For example, at an α-hederin/lipid ratio of 8, one population was centered at ∼70 nm and the other at ∼255 nm. At higher ratios, the samples presented a high polydispersity index, making the results unreliable. α-Hederin had a similar effect on LUVs composed of PC/SM/PI/Chol (4:4:3:5.5) (data not shown).

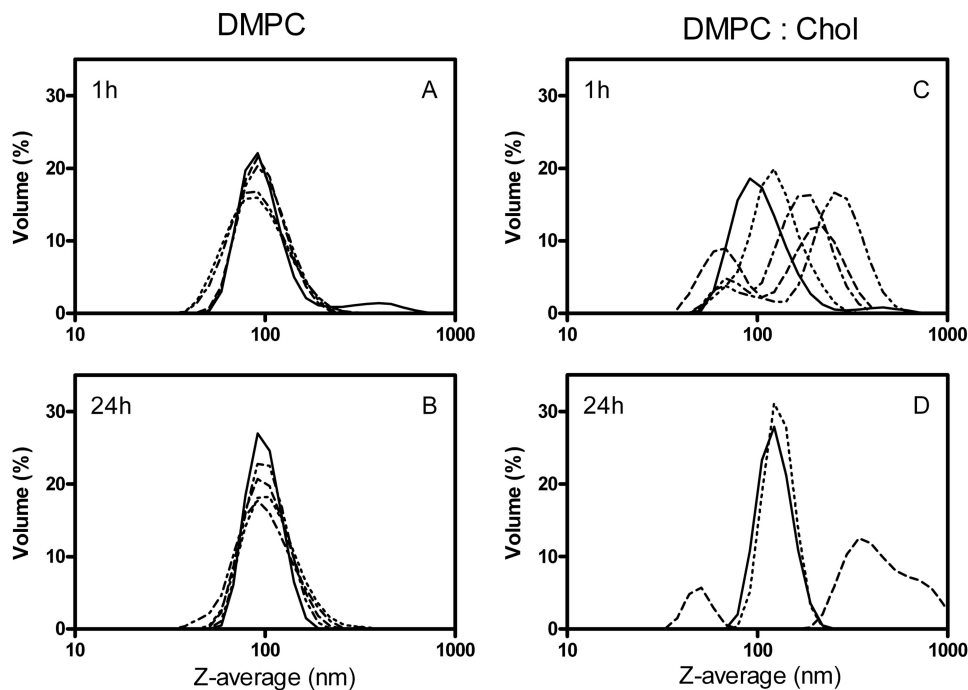Second, to gain information about the newly formed structures determined by dynamic light scattering, we used one-

FIGURE 6. **Z-average of liposomes upon exposure with α-hederin as determined by dynamic light scattering at high resolution in multimodal analysis.** Vesicles composed of DMPC (*A* and *B*) or DMPC/Chol (3:1) (*C* and *D*) were incubated for 1 h (*A* and *C*) or 24 h (*B* and *D*) without (*solid line*) or with α-hederin at a molar ratio of α-hederin/lipids of 1.2 (*dotted line*), 2.4 (*dashed line*), 4 (*dash dot line*), and 8 (*dash dot dot line*). For DMPC/Chol (3:1) vesicles, these ratios also correspond to α-hederin/cholesterol ratios of 4.8, 9.6, 16, and 32, respectively. For *D*, at α-hederin/lipid ratios higher than 2.4, the polydispersity index values became too high to have confident measures. The diameters of the particles are presented in nm, and the ordinate shows the volume of the population associated with a size expressed in %.

dimensional ^{31}P NMR spectroscopy. Fig. 7 shows the spectra of MLVs prepared with α-hederin (Fig. 7, *C–F*) and hederagenin (Fig. 7, *G–J*) at 10 (Fig. 7, *C, D, G,* and *H*) and 20% (Fig. 7, *E, F, I,* and *J*) mol/mol and at both 37 °C (*left column*) and 60 °C (*right column*).

DMPC/Chol (3:1) MLVs showed at 37 and 60 °C (Fig. 7, *A* and *B*) typical spectra of a bilayer organization displaying an asymmetric pattern with a low field shoulder and a high field peak. The chemical shift anisotropy (Δσ) was 40 and 39 ± 1 ppm. α-Hederin (10% mol/mol), at 37 °C (Fig. 7*C*), clearly disrupted the bilayer organization. The spectra showed a broad peak centered at 0 ppm superimposed to the bilayer shape. Δσ decreased from 40 ± 1 to 34.5 ± 1 ppm reflecting the presence of structures with higher mobility or diffusibility. At 60 °C, a sharp peak overlapping with a wide peak centered on 0 ppm became more pronounced, and a hexagonal phase pattern became noticeable (Fig. 7*D*). The Δσ reduction was similar to that observed at 37 °C (from 39 ± 1 to 33.5 ± 1 ppm). Macroscopically, for both temperatures, a phase separation was observed in the NMR tube as described in a system composed of bilayer/cubic and bilayer/hexagonal phases (44, 45). By increasing the α-hederin concentration to 20% mol/mol, at 37 °C, the bilayer structure was heavily disrupted because its characteristic asymmetrical peak has completely disappeared (Fig. 7*E*). A broad peak (over 10 ppm) centered at 0 ppm was observed in these conditions, which could correspond to structures larger than micelles like buds or small unilamellar vesicles, for example (46–48). By increasing the temperature to 60 °C (Fig. 7*F*), the one-dimensional ^{31}P NMR spectrum clearly showed a hexagonal pattern (highlighted by an *arrow* in Fig. 7*F′*). Macro-

scopically, the phase separation disappeared at high α-hederin concentration. The effects are critically dependent upon the presence of cholesterol because we did not observe any change in spectra, except a small increase of Δσ (39 to 42.5 ppm), when α-hederin (10%) was inserted in bilayers lacking cholesterol at 37 °C.

Hederagenin, at 10% mol/mol affected the bilayer signal to a lower extent compared with α-hederin. At 37 °C, the Δσ only decreased from 40 ± 1 to about 36.5 ± 1 ppm (Fig. 7*G*). As for α-hederin, a broad peak centered at 0 ppm was observed at 60 °C (Fig. 7*H*), and this peak increased with a concomitant decrease of the intensity of the bilayer signal. At a higher concentration (20% mol/mol) and both at 37 and 60 °C (Fig. 7, *I* and *J*), hederagenin induced a sharp isotropic peak at 0.4 ppm even though the bilayer signal was always present (Δσ = 38 ± 1 and 37 ± 1 ppm at 37 and 60 °C, respectively). We observed neither a significant change of Δσ nor a macroscopic phase separation regardless the concentrations tested.

This is in strict contrast with what was observed when SDS was used as a positive control. In these conditions, a reduction of Δσ to values to 29 and 26.5 ± 1 ppm at 37 and 60 °C, respectively, was observed with the appearance of a small isotropic peak at 0 ppm (see supplemental Fig. S3). This effect could be related to the size reduction of the vesicles induced by this detergent even though the bilayer structure is maintained (47). This mode of action is different from the one of α-hederin that deeply modifies the structure of the cholesterol containing MLVs.

In a nutshell, α-hederin did not change the mean diameter of the liposomes lacking cholesterol. When liposomes contained
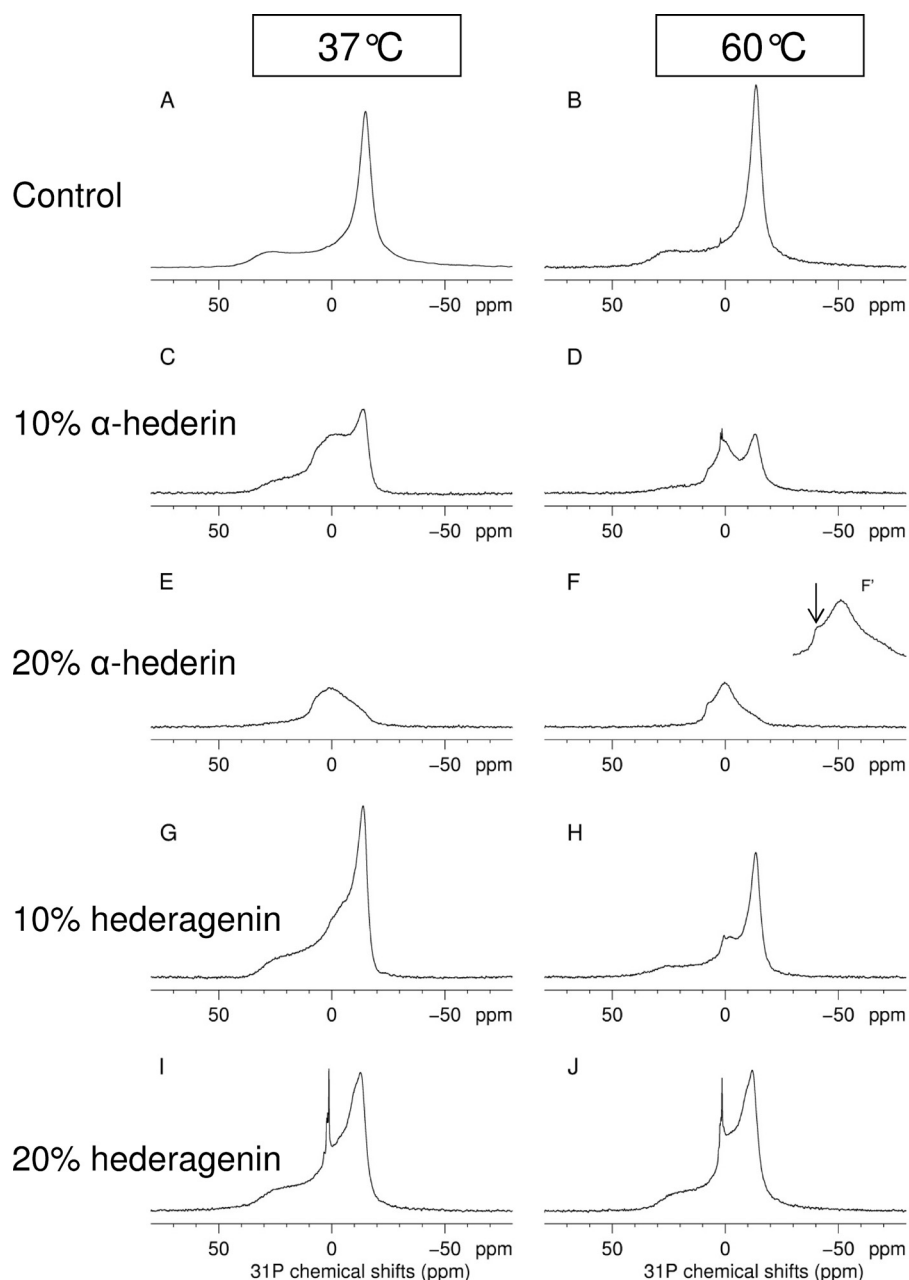
FIGURE 7. **^{31}P NMR spectra of MLVs composed of DMPC/cholesterol (3:1) at 37 °C (*left column*) or 60 °C (*right column*).** Control (*A* and *B*), 10% mol/mol α-hederin (*C* and *D*); 20% mol/mol α-hederin (*E–F′*); 10% mol/mol hederagenin (*G* and *H*), and 20% mol/mol hederagenin (*I* and *J*). 10 or 20% α-hederin or hederagenin corresponds to a molar ratio of compound/total lipids ratio = 0.1 or 0.2, respectively.

cholesterol, the saponin induced two new populations of different sizes most probably due to the formation of new lipid structures composed of a mixture of bilayers, isotropic and hexagonal phases. At higher α-hederin concentrations and temperatures, the hexagonal pattern was favored (see Fig. 7*F′*).

Packing at the Interfacial and Hydrophobic Regions of the Lipid Bilayer—To characterize the binding of α-hederin at the molecular level and particularly the consequences of its interaction within the interfacial domain, we determined GP_{ex}. A high GP_{ex} value is usually associated with a high bilayer packing and a low polarity and a low GP_{ex} value with the opposite (37). This was illustrated by changes in the decreasing GP_{ex} values upon increasing temperatures (Fig. 8). At physiological and

high temperatures, α-hederin and hederagenin induced a marked increase in GP_{ex} values on DMPC vesicles (Fig. 8, *A* and *B*).

When cholesterol was present in the liposomes (3:1), the trend of the curves was modified (Fig. 8, *C* and *D*) in accordance with other studies (49, 50). We observed a slight reduction of GP_{ex} values at low temperatures that became important at physiological temperatures (Fig. 8*C*). At higher temperatures, GP_{ex} increased as compared with the control situation, especially at the highest α-hederin/lipid ratio investigated. Hederagenin (Fig. 8*D*) had no effect at physiological temperature, but it induced a small decrease of the GP_{ex} below 40 °C and a slight increase above this temperature.
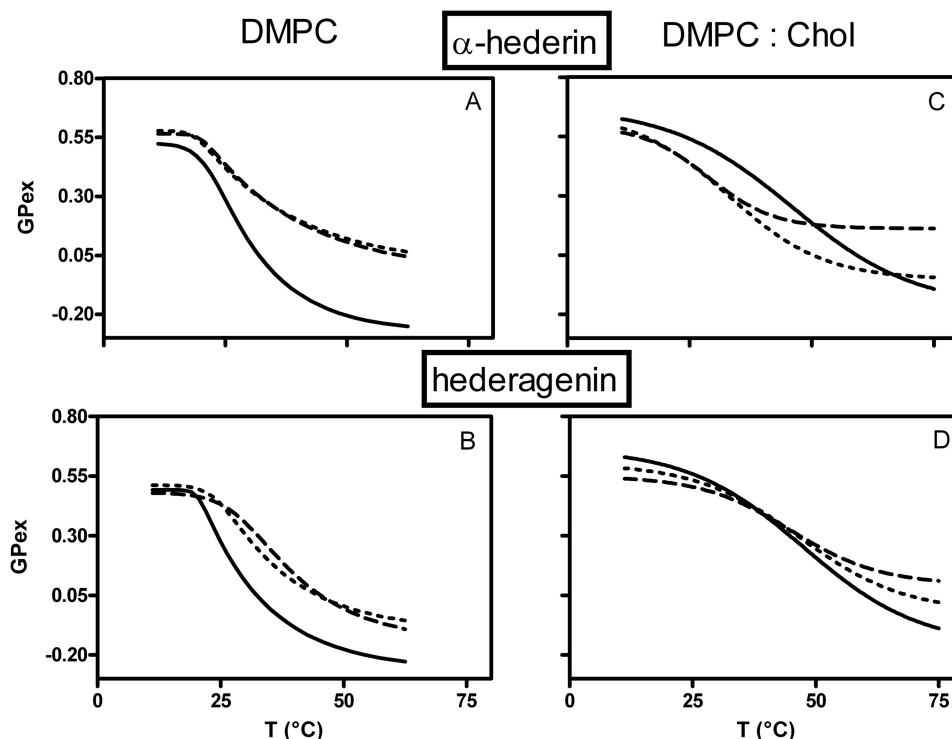
FIGURE 8. **Effect of α-hederin (A and C) and hederagenin (B and D) on the generalized polarization (GP$_{ex}$) values for laurdan in liposomes made of DMPC (A and B) or DMPC/Chol (3:1) (C and D) as a function of temperature.** The *lines* refer to data obtained in absence (*solid line*) or presence of α-hederin or hederagenin at drug/lipid molar ratios of 1.2 (*dotted line*) or 2.4 (*dashed line*). For DMPC/Chol (3:1) vesicles, these ratios correspond to a drug/cholesterol ratio of 4.8 and 9.6, respectively. The excitation wavelength was fixed at 340 nm and emission intensities at 440 nm (gel phase) and 490 nm (liquid crystalline phase). Each value is the average of three experiments. Statistical analysis was performed with Graph Pad Prism 4.0 (two-way ANOVA, comparing three data points at the beginning, physiological temperature, and the end of the curves).

Thus, at physiological conditions, and if cholesterol is present, only α-hederin induced a decrease of the GP$_{ex}$ values. At the highest temperatures investigated, both α-hederin and hederagenin increased GP$_{ex}$ values regardless of the presence of cholesterol. The same general observations for Laurdan GP$_{ex}$ have been made for DPH fluorescence anisotropy (*r*), a probe integrated into the hydrophobic core (data not shown).

Appearance of Membrane Deformations, Micrometric Pore Formation, and Budding—To ascertain the critical role of the sugars branched on the genin, we aimed to visualize the earliest alterations induced by α-hederin, δ-hederin, and hederagenin and their ability to promote shape deformations on GUVs containing cholesterol (16). An initial image was captured immediately after the addition of GUVs to the solution containing the compound. One GUV was followed over 60 min, and pictures were taken at regular time intervals. Images, presenting time intervals with important features, are shown in Fig. 9 upon addition of GUVs to a control solution (Fig. 9A) or to a solution containing α-hederin (Fig. 9B), δ-hederin (Fig. 9C), or hederagenin (Fig. 9D). The mean size diameter of GUVs at all times points was also monitored.

Just after their addition to a solution containing α-hederin (Fig. 9B), the GUVs possessed a spherical shape with no detectable membrane fluctuations. Then a rapid decrease in the mean diameter of the liposomes was observed (Fig. 9E), and after 30 min of incubation, wrinkled borders appeared. These wrinkles were more pronounced after 40 min (Fig. 9B, *white arrow*). Deformation was visible until 50 min but reversed to a spherical shape at 60 min. Quantification of wrinkled borders induced by

α-hederin is shown in Fig. 11 (85.2 ± 2.2% after 30 min (Fig. 11A) and 72.0 ± 17.2% after 1 h (Fig. 11B) of incubation).

With δ-hederin (Fig. 9C), wrinkled borders were much less present (4.7 ± 1.2% after 30 min (Fig. 11C) and 13.4 ± 6.2% after 1 h (Fig. 11D)). A marked decrease of the size of GUVs was observed but later (40 min), as compared with α-hederin (Fig. 9E).

Hederagenin induced neither membrane deformation (Fig. 9D) nor reduction in the size (Fig. 9E) of the GUVs, but sometimes it induced the formation of intravesicular buds (Fig. 9D).

After longer incubation periods of GUVs with α-hederin and δ-hederin, we observed the formation of visible pores (Fig. 10, A–D). We took advantage of confocal microscopy (Fig. 10B) and three-dimensional image reconstruction (Fig. 10C) to visualize the pore formation induced by α-hederin. Sometimes more than one pore was visible on one GUV. These pores expanded with time. The rim of the pore rolled itself up through the external side of the membrane (Fig. 10, A–C), resulting in the rolled rim shape as described by Sakuma *et al.* (16). When the complete vesicle had been "rolled up," the resulting form often resembled an angulated torus (Fig. 10, *complete transformation*). The appearance of micrometer-sized pores increased with incubation time (2.2 ± 2.3% after 30 min (Fig. 11A) and 4.3 ± 1.5% after 1 h (Fig. 11B)). For δ-hederin (Fig. 11D), this transformation was also visible but less frequent. No pore formation was observed with hederagenin. SDS at 30 mM induced the fast formation of macroscopic pores (supplemental Fig. S2, pores) and subsequent dissolution of the vesicle into small vesicles (supplemental Fig. S2, dissolution).
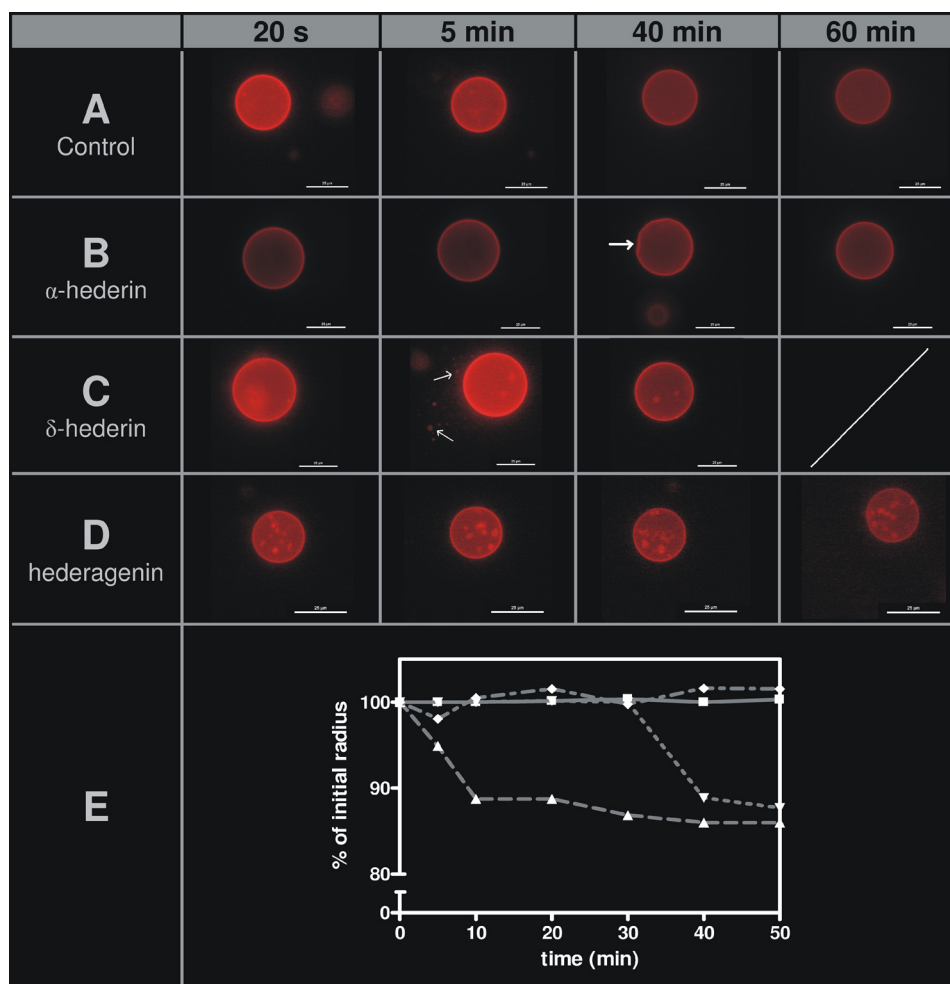
FIGURE 9. **Fluorescence microscopy of GUVs composed of DMPC/Chol (3:1) and labeled with TR-DPPE.** One GUV was followed, and pictures were taken at different incubation times. *A,* control; *B,* 40 μM α-hederin; *C,* 40 μM δ-hederin, and *D,* 40 μM hederagenin. One scale bar represents 25 μm. *E,* percentage of initial radius of one GUV as a function of incubation time with the compounds. The percentage was obtained by dividing the radius of a GUV at one time point by its radius measured when the incubation started. The ratio was multiplied by 100. Control liposomes (■), α-hederin (▲), δ-hederin (▼), and hederagenin (♦). The radius was determined using the acquisition software (see under "Experimental Procedures"). The experiment was performed three times at 25 °C. *Arrows* indicate deformation of the GUV for α-hederin and budding for δ-hederin.

Because the slight area difference between the two mono-layer leaflets of the membrane or a change in the vesicle area-to-volume ratio may lead to budding (51), we investigated the ability of α-hederin, δ-hederin, and hederagenin to induce budding again by using fluorescence (Fig. 10*E*) and confocal microscopy (Fig. 10*F*).

Because this process was mostly induced by δ-hederin, it has only been illustrated for this saponin (Fig. 10, *E* and *F*). Two different kinds of buddings were observed. First, immediate budding led to complete fission of the newly formed vesicle. Small fluorescent spheres were formed several minutes after incubation (Figs. 10, *immediate budding,* and 9*C, white arrows*). These spheres detached from the membrane, and a decrease in the mean diameter was observed after 40 min of incubation (Fig. 9*E*). Second, later budding, leading to incomplete fission, was produced at longer incubation periods, with the formation of larger vesicles, which were interconnected by nano-tubes and did not detach from the membrane (Fig. 10, *later budding*). With α-hederin, budding was occasionally only observed after 1 h of incubation (2.2 ± 1.4%; Fig. 11*B*), but with δ-hederin this process was much more frequent (23.4 ±

3.5% after 30 min (Fig. 11*C*) and 20.1 ± 5.3% after 1 h (Fig. 11*D*)). SDS (supplemental Fig. S2, budding) was also able to induce budding at concentrations of 400 μM, 4 mM, and 30 mM. The size of the buds decreased with increasing concentrations of SDS.

The possible effect of osmotic stress on this process is excluded because of the significantly low concentration of the compounds (~40 μM), which is orders of magnitude lower than the concentration of salt (a few millimolars) that has been reported to induce vesicle budding (52).

DISCUSSION

α-Hederin, a triterpenoid saponin, induced membrane permeabilization in relation to its biological activity. Despite numerous studies, the molecular mechanism involved remains unknown.

The results we obtained highlighted the role of a curvature-driven process (see Fig. 12), characterized by a three-step mechanism as follows: (i) cholesterol-independent binding to the membrane; (ii) interaction with cholesterol and asymmetric lateral distribution of α-hederin, and (iii) induction of curva-
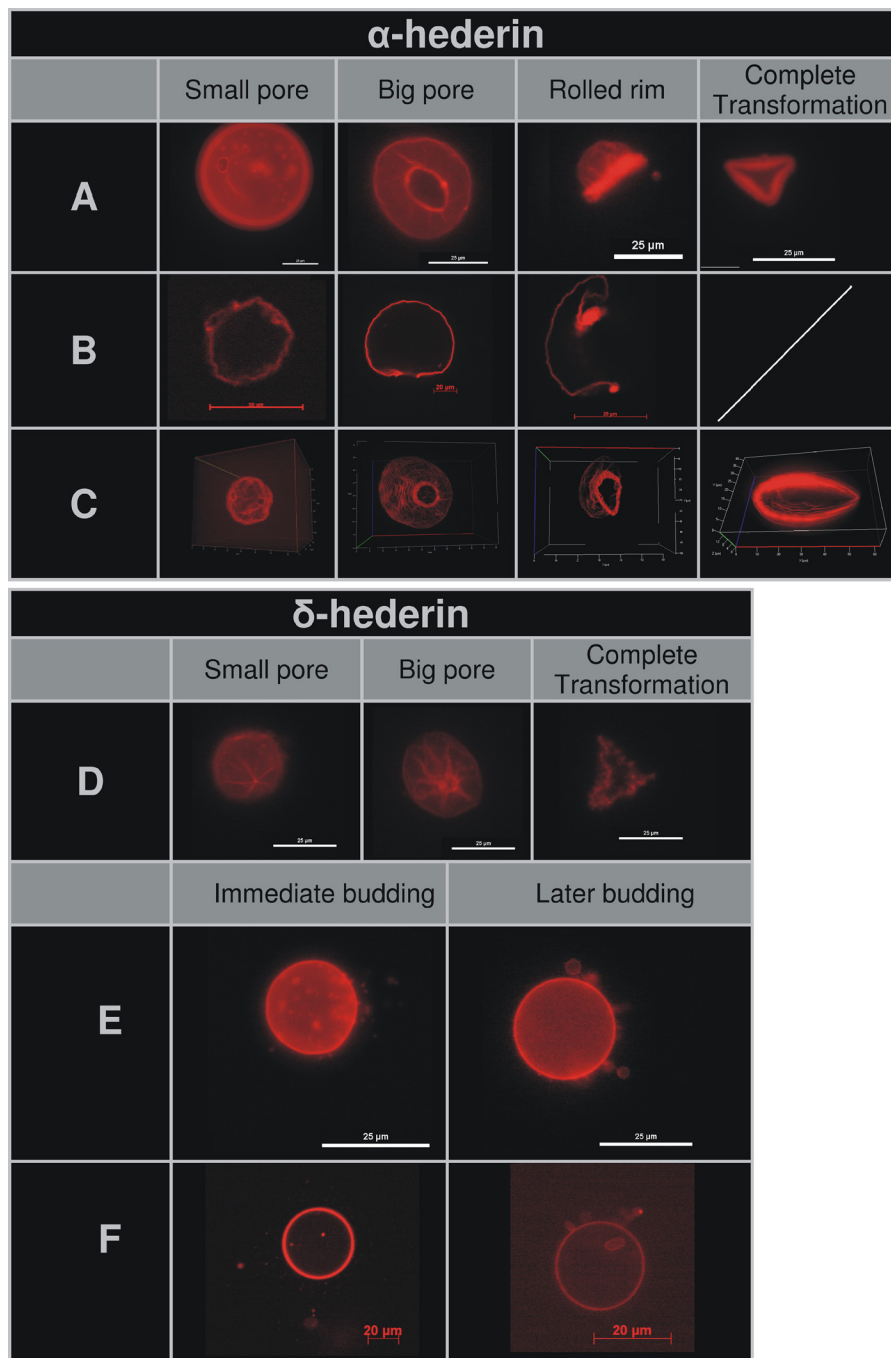
FIGURE 10. **Stages of pore formation (*A–D*) and budding (*E* and *F*) of GUVs composed of DMPC/Chol (3:1) incubated with 40 μM of α-hederin (*A–C*) or δ-hederin (*D–F*).** *A, D,* and *E,* fluorescence microscopy images of vesicles; *one bar* represents 25 μm. *B* and *F,* confocal microscopy, cross-section of the middle of one vesicle, *one bar* represents 20 μm. *C,* confocal microscopy, three-dimensional view of all cross-sections taken from one vesicle.

ture stress, resulting in membrane permeabilization and pore formation, as well as budding and the formation of a new lipid phase containing cholesterol, α-hederin, and phospholipids.

First, the cholesterol-independent binding of α-hederin and hederagenin to DMPC liposomes was suggested by the decrease in the membrane potential of lipid bilayers that could result from the negatively charged carboxylic function of the genin interacting with the positively charged choline head group of DMPC. Such interaction of α-hederin with the phospholipids results in an increase of the GP_{ex} of laurdan, especially at physiological and high temperatures. This suggests an increase in the microviscosity at the level of the polar heads of DMPC. A similar effect was observed for α-hederin when the hydrophobic membrane core was investigated. Condensing and acyl chain ordering effects on the phospholipids in their liquid disordered (L_d) state are similar to the effects that have been well described for cholesterol and assigned to the rigid ring structure of the sterol limiting trans $\rightarrow$ gauche isomerization of vicinal phospholipid acyl chains (53). Thus, the rigid triterpenoid structure of the genin could explain our results because both α-hederin and hederagenin are able to increase the GP_{ex} in the absence of cholesterol.
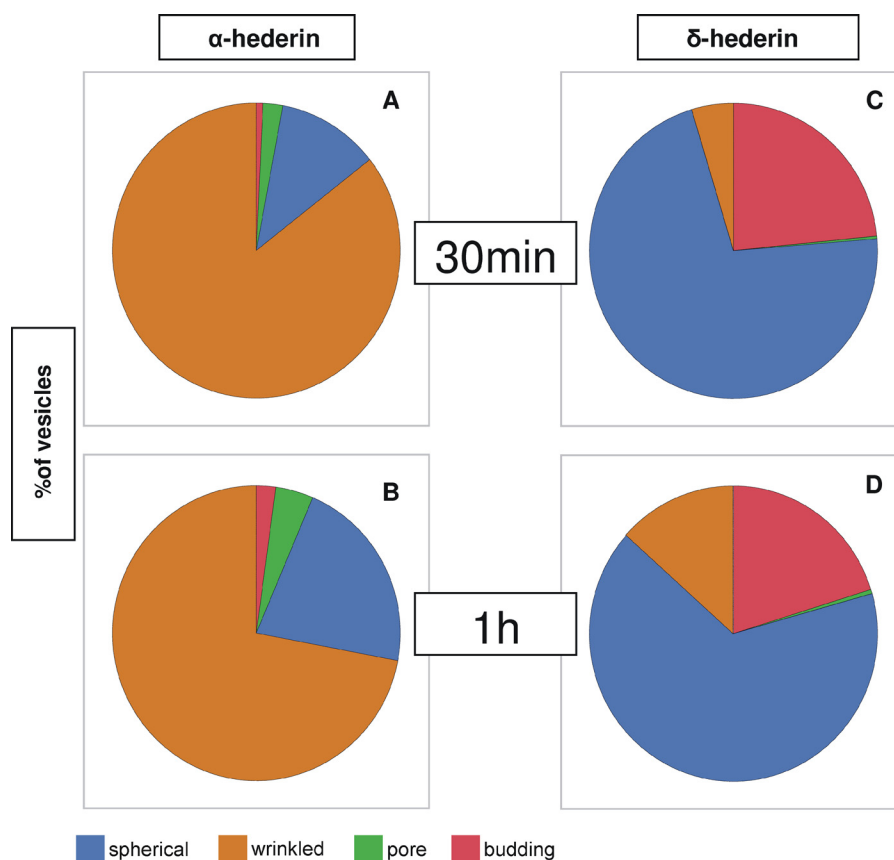
FIGURE 11. **Quantification of vesicles presenting different features (spherical, wrinkled, pores, or budding) after 30 min of incubation (*A* and *C*) or 1 h of incubation (*B* and *D*) with 40 μM of α-hederin (*A* and *B*) or δ-hederin (*C* and *D*).** A total of 200 vesicles were counted.

Second, after the initial binding to lipid membranes (Fig. 12*B*), α-hederin would interact with cholesterol, inducing a marked decrease of GP_{ex} values at physiological temperatures in DMPC/Chol (3:1). The formation of equimolecular complexes or aggregates composed of cholesterol and saponins could disorganize the phospholipid/cholesterol matrix and change the thermotropic behavior of membranes (54, 55). Our results from DHE spectroscopy support such interaction between cholesterol and α-hederin. Hederagenin only slightly influenced GP_{ex}, leading to the assumption that the decrease of GP_{ex} is mainly dependent on the sugar residues. The glycoside residues could act like "umbrellas," shielding the nonpolar part of cholesterol from water (56), and thereby enhancing the interaction between the saponin and the sterol (Fig. 12*B*) and inhibiting polar interactions of the phospholipids with the sterols.

Third, α- and δ-hederin would induce permeabilization of LUVs and GUVs, as well as the formation of wrinkles, micrometer-sized pores and buds in GUV, as well as the formation of a new lipid phase in MLVs. All these effects are highly dependent upon the nature of the saponin (α-hederin, δ-hederin, or hederagenin).

The appearance of GUVs presenting a flaccid shape and wrinkling would most likely result from the inhomogeneous insertion of saponin molecules and the release of the intravesicular Laplace pressure and internal water after permeabilization (57). The flaccid-shaped vesicles sometimes redeveloped into a spherical vesicle, with a smaller radius, suggesting a loss of membrane material, which could be related to the formation

of the new isotropic lipid phase as evidenced by ^{31}P NMR spectroscopy and suggested by DHE spectroscopy on MLVs. This new phase would most probably be composed of cholesterol, α-hederin, and DMPC.

Budding and permeabilization have been previously associated with changes in surface area and spontaneous curvature (58–63). At first glance, the effects of the area asymmetry resulting from the bending of the inner monolayer after the insertion of molecules in the outer monolayer and an increase in the surface area (62–63) should be stronger than the effects of the spontaneous curvatures. However, with compounds characterized by a cone shape (like for α-hederin) or an inverted cone shape, which are locally accumulated, the opposite takes place, with the effects of spontaneous curvature being stronger than those of the area asymmetry. Thus, relative changes in the local lipid composition would result in the variation of the bilayer spontaneous curvature in the same location, making this mechanism more effective than that based on the area difference averaged over the entire membrane surface (60).

The induction of spontaneous curvature induced by α-hederin is supported by the following: (i) nonbilayer structures with a higher rate of Brownian tumbling or lateral diffusion around the vesicle observed by ^{31}P NMR (64, 65) in accordance with the reduction of the chemical shift anisotropy; (ii) the new structures of different sizes evidenced by dynamic light scattering; (iii) the decrease of GP_{ex} and DPH fluorescence anisotropy values observed at 37 °C (42, 63); (iv) the formation of macroscopic pores (16), and (v) budding (66).
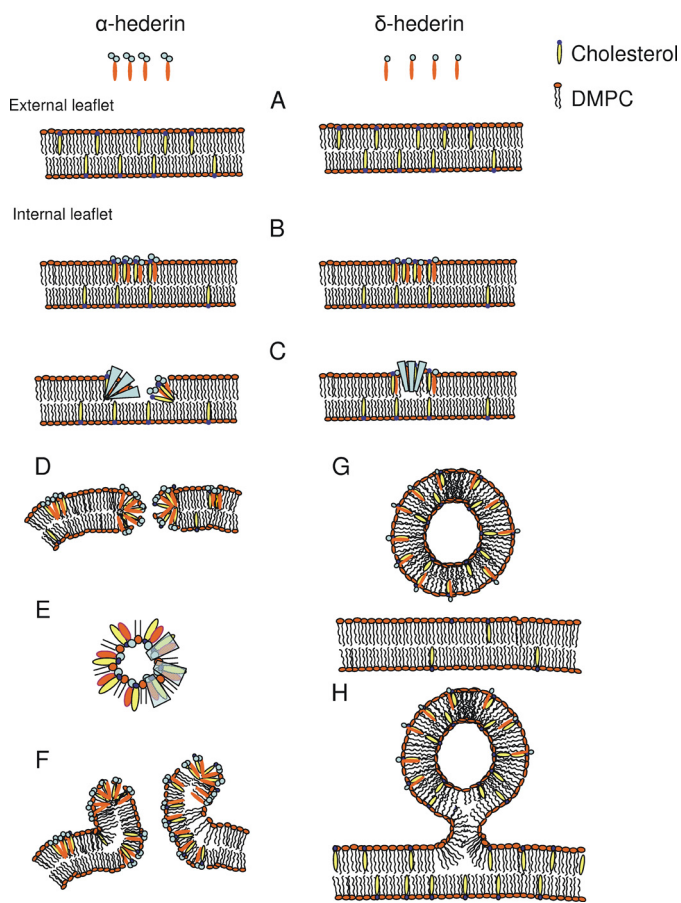
FIGURE 12. **Model proposed for the interaction of α-hederin and δ-hederin with GUVs.** *A,* α-hederin binds independently of cholesterol to the membrane and integrates into the outer leaflet. *B,* interaction between saponins and cholesterol leads to the formation of regions with a higher α- and δ-hederin/cholesterol concentration. *C,* increase of spontaneous curvature in a transbilayer direction due to the sugar moiety of the saponin in these regions leads to permeabilization (*D*) or budding (*G* and *H*). *D,* pore is stabilized by the sugar moieties pointing to the exterior of the membrane and reducing line tension, and a slight negative curvature in the direction of the membrane plane (*E*). *F,* diffusion of α-hederin at the rim toward the interior of the vesicle leads to inhomogeneous distribution of α-hederin molecules between the inner and outer leaflet and the rolled rim shape. *G* and *H,* intermediate curvature of δ-hederin is responsible for the immediate budding with complete fission from the GUVs at the beginning of incubation (*G*) and for the later budding with the bud still connected to the GUV at longer incubation times (*H*).

The nature of the formed nonbilayer structures is unknown, and electron or atomic force microscopy would have to be performed to fully characterize the structures. Among the more mobile structures, which could be induced by α-hederin, cubic phases or structures larger than micelles, like *e.g.* buds or small unilamellar vesicles (46–48, 67), are the most likely. The hexagonal pattern observed at the highest temperature and α-hederin concentration could probably be associated with tubular structures as it has been suggested for glycoalkaloids (10).

The enhancement of curved structures in relation to membrane permeabilization appears clearly related to the nature of the saponin (α-hederin, δ-hederin, and hederagenin). In agreement with the self-assembly theory established by Israelachvili *et al.* (68), amphiphiles are approximated by rigid bodies of defined three-dimensional shape (Fig. 1). α-Hederin has two sugar units, which confer to the molecule a large hydrophilic headgroup compared with its lipophilic, rigid triterpenic pen-

tacyclic ring structure, which results in a positive spontaneous curvature, as it adopts a cone shape. The sugar moiety points in the direction perpendicular to the genin, giving the molecule the form of an axe. The formation of a normal hexagonal phase (H_I) (or tubular structures) would be in accordance with the three-dimensional shape proposed for α-hederin (very slight curvature in one direction and positive curvature into the other) (60). In this context, toroidal pore formation has been associated with a positive spontaneous curvature applied to the transbilayer direction and negative curvature regarding the rim of the pore in the membrane plane (69, 70). Aggregation of cholesterol and α-hederin could lead to a complex presenting positive curvature (cone shape) in a transbilayer direction and slight negative curvature (inverted truncated cone shape) in the membrane plane (Fig. 12, *D* and *E*).

δ-Hederin has only one sugar at C3. Its hydrophilic headgroup is smaller and the positive spontaneous curvature applied should decrease relative to α-hederin. δ-Hederin would induce smaller positive curvatures into the transbilayer direction. Hederagenin has a structure that resembles cholesterol, and its spontaneous curvature should therefore be negative, as has been observed for cholesterol (57), explaining its lower ability to induce pore formation.

SDS, a molecule with a single acyl chain and an ionized sulfate group, would rather induce positive curvature in all directions of the membrane plane. This would lead to the formation of pores, small buds, and/or micelles, which is in accordance with our results. The critical role of a three-dimensional molecular shape and the ability to induce curvature have also been proposed to explain membrane permeabilization induced by the following: (i) dioscin (71); (ii) glycoalkaloids (10); (iii) cone-shaped amphiphiles (57), and (iv) cone-shaped lipids (16).

Regarding the kinetics of pore formation, the permeabilization to 4-kDa FITC-dextran was faster than to 250-kDa FITC-dextran. Moreover, an increase in the time to reach micrometer-sized pores was observed, as reported when hepatocytes were treated with saponins extracted from *Gypsophila* plants (72). Therefore, permeabilization appeared to be a graded process, characterized by the appearance of wrinkled borders and the continuing shape deformations, as well as the formation of pores with increasing size. For influx to occur, the pores should be equal to or larger than the Stokes-Einstein radii of FITC-dextran molecules (73) (1.83 and 11.1 nm for 4- and 250-kDa FITC-dextran, respectively). With time, the pores were stabilized, and the formation of the so-called rolled-rim shape was observed (16). The segregated cone-shaped amphiphilic α-hederin molecules could cap the edge of the bilayer at the rim of the pore, decreasing line tension and thereby stabilizing the pore (16, 57). The membrane at the rim was rolled to the outside of the vesicle after pore formation (Fig. 10, *rolled rim*; Fig. 12*F*), which could result from a time-dependent inhomogeneous distribution of saponin molecules between the inner and outer leaflet, a model that has been recently established for cone-shaped amphiphiles (16).

As membrane permeabilization, budding is favored by molecules that induce positive curvature to the external monolayer (Fig. 12, *C, G,* and *H*). Immediate budding (Figs. 9 and 10) occurred just after the GUVs had been added to the δ-hederin

solution. At this stage, we observed no permeabilization of the GUV to dextran. GUVs behaved in exactly the same manner in a SDS solution. Because of its hydrophilic sugar moiety, we can assume that δ-hederin will not flip to the internal monolayer and only induce positive curvature to the external leaflet that would result mostly in budding. The buds were variable in size, suggesting differences in concentrations of δ-hederin in the external monolayer of the vesicles. These buds detached from the membrane and created independent spheres or, upon increasing incubation time, formed pearled structures (buds connected through necks (Fig. 10*H*), later budding) as observed with low concentrations of detergents or lysophosphatidylcholines (66, 74). GUVs in the presence of hederagenin formed intravesicular buds, which is in accordance with the inverted cone shape and resulting negative curvature of this molecule.

In addition to the mechanism of permeabilization induced by α-hederin, the importance of cholesterol concentration within the membrane must be discussed. Calcein release from LUV demonstrated that α-hederin induced no permeabilization in membranes lacking cholesterol, even at a concentration reaching its solubility limit (data not shown). It appears that a certain cholesterol density in the liposomes is required to allow α-hederin to induce pores. The importance of this threshold for pore formation by other saponins agrees with observations reported by others (9, 10, 75, 76). On cells, THP-1 macrophages depleted in cholesterol were protected against cytotoxicity induced by α-hederin. This ascertained the physiological relevance of our work, and the high amounts of cholesterol especially in resistant cancer cell lines could confer some specificity to α-hederin derivatives or similar saponins toward these cells (77, 78). Very rapid cell death was obtained at high concentrations of α-hederin. Gauthier *et al.* (5) showed that α-hederin would induce cancer cell death to a large extent by membrane permeabilization, and similar to our results, they showed that α-hederin was more effective in inducing membrane permeabilization than δ-hederin, whereas hederagenin had no effect on three different cancer cell lines.

In conclusion, this work contributes to the understanding of the mechanism involved in membrane disruption induced by α-hederin and δ-hederin, and other monodesmosidic saponins. It demonstrates the role of cholesterol in this process and shows the effect of the sugar moieties branched on the genin on permeabilization. Understanding the molecular mechanism involved in membrane permeabilization is critical and can be exploited for therapeutic applications, such as the development of pore-forming proteins or peptide-based antibiotics and the design of membrane-permeabilizing drugs that selectively kill cancer cells (79).

REFERENCES

1. Francis, G., Kerem, Z., Makkar, H. P., and Becker, K. (2002) The biological action of saponins in animal systems: a review. *Br. J. Nutr.* **88,** 587–605
2. Choi, J. H., Lee, H. W., Park, H. J., Kim, S. H., and Lee, K. T. (2008) Kalopanaxsaponin A induces apoptosis in human leukemia U937 cells through extracellular Ca²⁺ influx and caspase-8 dependent pathways. *Food Chem. Toxicol.* **46,** 3486–3492
3. van der Haar, A. W. (1912) Phytochemische untersuchungen in der familie der Araliaceae. I. Saponinartige glykoside aus polyscias nodosa und hedera helix. *Arch. Pharm.* **250,** 560
4. Chwalek, M., Lalun, N., Bobichon, H., Plé, K., and Voutquenne-Nazabadioko, L. (2006) Structure-activity relationships of some hederagenin diglycosides: haemolysis, cytotoxicity, and apoptosis induction. *Biochim. Biophys. Acta* **1760,** 1418–1427
5. Gauthier, C., Legault, J., Girard-Lalancette, K., Mshvildadze, V., and Pichette, A. (2009) Haemolytic activity, cytotoxicity, and membrane cell permeabilization of semi-synthetic and natural lupane- and oleanane-type saponins. *Bioorg. Med. Chem.* **17,** 2002–2008
6. Swamy, S. M., and Huat, B. T. (2003) Intracellular glutathione depletion and reactive oxygen species generation are important in α-hederin-induced apoptosis of P388 cells. *Mol. Cell. Biochem.* **245,** 127–139
7. Kumara, S. S., and Huat, B. T. (2001) Extraction, isolation, and characterisation of antitumor principle, α-hederin, from the seeds of *Nigella sativa. Planta Med.* **67,** 29–32
8. Danloy, S., Quetin-Leclercq, J., Coucke, P., De Pauw-Gillet, M. C., Elias, R., Balansard, G., Angenot, L., and Bassleer, R. (1994) Effects of α-hederin, a saponin extracted from hedera helix, on cells cultured in vitro. *Planta Med.* **60,** 45–49
9. Armah, C. N., Mackie, A. R., Roy, C., Price, K., Osbourn, A. E., Bowyer, P., and Ladha, S. (1999) The membrane-permeabilizing effect of avenacin A-1 involves the reorganization of bilayer cholesterol. *Biophys. J.* **76,** 281–290
10. Keukens, E. A., de Vrije, T., van den Boom, C., de Waard, P., Plasman, H. H., Thiel, F., Chupin, V., Jongen, W. M., and de Kruijff, B. (1995) Molecular basis of glycoalkaloid-induced membrane disruption. *Biochim. Biophys. Acta* **1240,** 216–228
11. Mouritsen, O. G., and Zuckermann, M. J. (2004) What's so special about cholesterol? *Lipids* **39,** 1101–1113
12. Sieben, A., Prenner, L., Sorkalla, T., Wolf, A., Jakobs, D., Runkel, F., and Häberlein, H. (2009) α-Hederin, but not hederacoside C and hederagenin from hedera helix, affects the binding behavior, dynamics, and regulation of β2-adrenergic receptors. *Biochemistry* **48,** 3477–3482
13. Kerdous, R., Heuvingh, J., and Bonneau, S. (2011) Photo-dynamic induction of oxidative stress within cholesterol-containing membranes: shape transitions and permeabilization. *Biochim. Biophys. Acta* **1808,** 2965–2972
14. Tamba, Y., Ariyama, H., Levadny, V., and Yamazaki, M. (2010) Kinetic pathway of antimicrobial peptide magainin 2-induced pore formation in lipid membranes. *J. Phys. Chem. B* **114,** 12018–12026
15. Wesołowska, O., Michalak, K., Maniewska, J., and Hendrich, A. B. (2009) Giant unilamellar vesicles–a perfect tool to visualize phase separation and lipid rafts in model systems. *Acta Biochim. Pol.* **56,** 33–39
16. Sakuma, Y., Taniguchi, T., and Imai, M. (2010) Pore formation in a binary giant vesicle induced by cone-shaped lipids. *Biophys. J.* **99,** 472–479
17. Chong, P. L., and Wong, P. T. (1993) Interactions of Laurdan with phosphatidylcholine liposomes: a high pressure FTIR study. *Biochim. Biophys. Acta* **1149,** 260–266
18. Kaiser, R. D., and London, E. (1998) Location of diphenylhexatriene (DPH) and its derivatives within membranes: comparison of different fluorescence quenching analyses of membrane depth. *Biochemistry* **37,** 8180–8190
19. Lentz, B. R. (1993) Use of fluorescent probes to monitor molecular order and motions within liposome bilayers. *Chem. Phys. Lipids* **64,** 99–116
20. Shinitzky, M., and Barenholz, Y. (1978) Fluidity parameters of lipid regions determined by fluorescence polarization. *Biochim. Biophys. Acta* **515,** 367–394
21. Van Bambeke, F., Mingeot-Leclercq, M. P., Schanck, A., Brasseur, R., and

Tulkens, P. M. (1993) Alterations in membrane permeability induced by aminoglycoside antibiotics–Studies on liposomes and cultured cells. *Eur. J. Pharmacol.* **247,** 155–168

22. Christian, A. E., Haynes, M. P., Phillips, M. C., and Rothblat, G. H. (1997) Use of cyclodextrins for manipulating cellular cholesterol content. *J. Lipid Res.* **38,** 2264–2272

23. Bensikaddour, H., Snoussi, K., Lins, L., Van Bambeke, F., Tulkens, P. M., Brasseur, R., Goormaghtigh, E., and Mingeot-Leclercq, M. P. (2008) Interactions of ciprofloxacin with DPPC and DPPG: fluorescence anisotropy, ATR-FTIR, and 31P NMR spectroscopies and conformational analysis. *Biochim. Biophys. Acta* **1778,** 2535–2543

24. Hope, M. J., Bally, M. B., Webb, G., and Cullis, P. R. (1985) Production of large unilamellar vesicles by a rapid extrusion procedure–Characterization of size distribution, trapped volume, and ability to maintain a membrane potential. *Biochim. Biophys. Acta* **812,** 55–65

25. Bartlett, G. R. (1959) Phosphorus assay in column chromatography. *J. Biol. Chem.* **234,** 466–468

26. Weinstein, J. N., Yoshikami, S., Henkart, P., Blumenthal, R., and Hagins, W. A. (1977) Liposome-cell interaction: transfer and intracellular release of a trapped fluorescent marker. *Science* **195,** 489–492

27. Lelkes, P. I. (1984) in *Liposome Technology* (Gregoriadis, G., ed) Vol. 3, p. 225, CRC Press, Inc., Boca Raton, FL

28. Domenech, O., Francius, G., Tulkens, P. M., Van Bambeke, F., Dufrêne, Y., and Mingeot-Leclercq, M. P. (2009) Interactions of oritavancin, a new lipoglycopeptide derived from vancomycin, with phospholipid bilayers: Effect on membrane permeability and nanoscale lipid membrane organization. *Biochim. Biophys. Acta* **1788,** 1832–1840

29. Loura, L. M., and Prieto, M. (1997) Dehydroergosterol structural organization in aqueous medium and in a model system of membranes. *Biophys. J.* **72,** 2226–2236

30. Wüstner D. (2007) Fluorescent sterols as tools in membrane biophysics and cell biology. *Chem. Phys. Lipids* **146,** 1–25

31. Cheng, K. H., Virtanen, J., and Somerharju, P. (1999) Fluorescence studies of dehydroergosterol in phosphatidylethanolamine/phosphatidylcholine bilayers. *Biophys. J.* **77,** 3108–3119

32. Seras, M., Gallay, J., Vinvent, M., Ollivon, M., and Lesieur, S. (1994) Micelle-vesicle transition of nonionic surfactant-cholesterol assemblies induced by octyl glucoside: a time-resolved fluorescence study of dehydroergosterol. *J. Colloid Interface Sci.* **167,** 159–171

33. Ma, J. Y., Ma, J. K., and Weber, K. C. (1985) Fluorescence studies of the binding of amphiphilic amines with phospholipids. *J. Lipid Res.* **26,** 735–744

34. Montero, M. T., Pijoan, M., Merino-Montero, S., Vinuesa, T., and Hernández-Borrell, J. (2006) Interfacial membrane effects of fluoroquinolones as revealed by a combination of fluorescence binding experiments and atomic force microscopy observations. *Langmuir* **22,** 7574–7578

35. Domenech, O., Dufrêne, Y. F., Van Bambeke, F., Tukens, P. M., and Mingeot-Leclercq, M. P. (2010) Interactions of oritavancin, a new semi-synthetic lipoglycopeptide, with lipids extracted from *Staphylococcus aureus*. *Biochim. Biophys. Acta.* **1798,** 1876–1885

36. Nazari, M., Kurdi, M., and Heerklotz, H. (2012) Classifying surfactants with respect to their effect on lipid membrane order. *Biophys. J.* **102,** 498–506

37. Parasassi, T., De Stasio, G., d'Ubaldo, A., and Gratton, E. (1990) Phase fluctuation in phospholipid membranes revealed by Laurdan fluorescence. *Biophys. J.* **57,** 1179–1186

38. Giraldo, J., Vivas, N. M., Vila, E., and Badia, A. (2002) Assessing the (a)symmetry of concentration-effect curves: empirical versus mechanistic models. *Pharmacol. Ther.* **95,** 21–45

39. Angelova, M. I., Soléau, S., Méléard, P., Faucon, J. F., and Bothorel, P. (1992) Preparation of giant vesicles by external AC electric fields. Kinetics and applications. *Prog. Colloid Polymer Sci.* **89,** 127–131

40. Juhasz, J., Davis, J. H., and Sharom, F. J. (2010) Fluorescent probe partitioning in giant unilamellar vesicles of "lipid raft" mixtures. *Biochem. J.* **430,** 415–423

41. Praper, T., Sonnen, A., Viero, G., Kladnik, A., Froelich, C. J., Anderluh, G., Dalla Serra, M., and Gilbert, R. J. (2011) Human perforin employs different avenues to damage membranes. *J. Biol. Chem.* **286,** 2946–2955

42. Luckey, M. (2008) *Structural Biology: With Biochemical and Biophysical Foundations*, pp. 13–41, Cambridge University Press, New York

43. van Meer, G. (2005) Cellular lipidomics. *EMBO J.* **24,** 3159–3165

44. Lohner, K., and Prenner, E. J. (1999) Differential scanning calorimetry and x-ray diffraction studies of the specificity of the interaction of antimicrobial peptides with membrane-mimetic systems. *Biochim. Biophys. Acta.* **1462,** 141–156

45. Kleinschmidt, J. H., and Tamm, L. K. (2002) Structural transitions in short-chain lipid assemblies studied by 31P NMR spectroscopy. *Biophys. J.* **83,** 994–1003

46. Viseu, M. I., Correia, R. F., and Fernandes, A. C. (2010) Time evolution of the thermotropic behavior of spontaneous liposomes and disks of the DMPC-DTAC aqueous system. *J. Colloid Interface Sci.* **351,** 156–165

47. King, M. D., and Marsh, D. (1989) Polymorphic phase behavior of lysopalmitoylphosphatidylcholine in poly(ethylene glycol)-water mixtures. *Biochemistry* **28,** 5643–5647

48. Nezil, F. A., Bayerl, S., and Bloom, M. (1992) Temperature-reversible eruptions of vesicles in model membranes studied by NMR. *Biophys. J.* **61,** 1413–1426

49. Parasassi, T., De Stasio, G., Ravagnan, G., Rusch, R. M., and Gratton, E. (1991) Quantitation of lipid phases in phospholipid vesicles by the generalized polarization of Laurdan fluorescence. *Biophys. J.* **60,** 179–189

50. Parasassi, T., Giusti, A. M., Raimondi, M., and Gratton, E. (1995) Abrupt modifications of phospholipid-bilayer properties at critical cholesterol concentrations. *Biophys. J.* **68,** 1895–1902

51. Käs, J., and Sackmann, E. (1991) Shape transitions and shape stability of giant phospholipid vesicles in pure water induced by area-to-volume changes. *Biophys. J.* **60,** 825–844

52. Hamada, T., Miura, Y., Ishii, K., Araki, S., Yoshikawa, K., Vestergaard, M., and Takagi, M. (2007) Dynamic processes in endocytic transformation of a raft-exhibiting giant liposome. *J. Phys. Chem. B* **111,** 10853–10857

53. Róg, T., Pasenkiewicz-Gierula, M., Vattulainen, I., and Karttunen, M. (2009) Ordering effects of cholesterol and its analogues. *Biochim. Biophys. Acta* **1788,** 97–121

54. Nishikawa, M., Nojima, S., Akiyama, T., Sankawa, U., and Inoue, K. (1984) Interaction of digitonin and its analogs with membrane cholesterol. *J. Biochem.* **96,** 1231–1239

55. Bangham, A. D., Horne, R. W., Glauert, A. M., Dingle, J. T., and Lucy, J. A. (1962) Action of saponin on biological cell membranes. *Nature* **196,** 952–955

56. Huang, J., and Feigenson, G. W. (1999) A microscopic interaction model of maximum solubility of cholesterol in lipid bilayers. *Biophys. J.* **76,** 2142–2157

57. Karatekin, E., Sandre, O., Guitouni, H., Borghi, N., Puech, P. H., and Brochard-Wyart, F. (2003) Cascades of transient pores in giant vesicles: line tension and transport. *Biophys. J.* **84,** 1734–1749

58. Lee, M. T., Hung, W. C., Chen, F. Y., and Huang, H. W. (2008) Mechanism and kinetics of pore formation in membranes by water-soluble amphipathic peptides. *Proc. Natl. Acad. Sci. U.S.A.* **105,** 5087–5092

59. Sudbrack, T. P., Archilha, N. L., Itri, R., and Riske, K. A. (2011) Observing the solubilization of lipid bilayers by detergents with optical microscopy of GUVs. *J. Phys. Chem. B* **115,** 269–277

60. Zimmerberg, J., and Kozlov, M. M. (2006) How proteins produce cellular membrane curvature. *Nat. Rev. Mol. Cell Biol.* **7,** 9–19

61. van Duyl, B. Y., Meeldijk, H., Verklej, A. J., Rijkers, D. T., Chupin, V., de Kruijff, B., and Killian, J. A. (2005) A synergistic effect between cholesterol and tryptophan-flanked transmembrane helices modulates membrane curvature. *Biochemistry* **44,** 4526–4532

62. Heinrich, V. V., Svetina, S., and Zeks, B. (1993) Nonaxisymmetric vesicle shapes in a generalized bilayer-couple model and the transition between oblate and prolate axisymmetric shapes. *Phys. Rev. E. Stat. Phys. Plasmas Fluids Relat. Interdiscip. Topics* **48,** 3112–3123

63. Sheetz, M. P., and Singer, S. J. (1974) Biological membranes as bilayer couples. A molecular mechanism of drug-erythrocyte interactions. *Proc. Natl. Acad. Sci. U.S.A.* **71,** 4457–4461

64. McLaughlin, A. C., Cullis, P. R., Hemminga, M. A., Hoult, D. I., Radda, G. K., Ritchie, G. A., Seeley, P. J., and Richards, R. E. (1975) Application of 31P NMR to model and biological membrane systems. *FEBS Lett.* **57,**

213–218

65. Cullis, P. R., De Kruyff, B., and Richards, R. E. (1976) Factors affecting the motion of the polar headgroup in phospholipid bilayers. A ^{31}P NMR study of unsonicated phosphatidylcholine liposomes. *Biochim. Biophys. Acta* **426,** 433–446

66. Allain, J. M., and Ben Amar, M. (2006) Budding and fission of a multiphase vesicle. *Eur. Phys. J. E. Soft. Matter* **20,** 409–420

67. Alves, I. D., Goasdoué, N., Correia, I., Aubry, S., Galanth, C., Sagan, S., Lavielle, S., Chassaing, G. (2008) Membrane interaction and perturbation mechanisms induced by two cationic cell penetrating peptides with distinct charge distribution. *Biochim. Biophys. Acta* **1780,** 948–959

68. Israelachvili, J. N., Mitchell, D. J., and Ninham, B. W. (1977) Theory of self-assembly of lipid bilayers and vesicles. *Biochim. Biophys. Acta* **470,** 185–201

69. Matsuzaki, K., and Horikiri, C. (1999) Interactions of amyloid β-peptide (1–40) with ganglioside-containing membranes. *Biochemistry* **38,** 4137–4142

70. Valcarcel, C. A., Dalla Serra, M., Potrich, C., Bernhart, I., Tejuca, M., Martinez, D., Pazos, F., Lanio, M. E., and Menestrina, G. (2001) Effects of lipid composition on membrane permeabilization by sticholysin I and II, two cytolysins of the sea anemone *Stichodactyla helianthus*. *Biophys. J.* **80,** 2761–2774

71. Lin, F., and Wang, R. (2010) Hemolytic mechanism of dioscin proposed by molecular dynamics simulations. *J. Mol. Model* **16,** 107–118

72. Wassler, M., Jonasson, I., Persson, R., and Fries, E. (1987) Differential permeabilization of membranes by saponin treatment of isolated rat hepatocytes. Release of secretory proteins. *Biochem. J.* **247,** 407–415

73. Venturoli, D., and Rippe, B. (2005) Ficoll and dextran *vs.* globular proteins as probes for testing glomerular permselectivity: effects of molecular size, shape, charge, and deformability. *Am. J. Physiol. Renal Physiol.* **288,** F605–F613

74. Tanaka, T., Sano, R., Yamashita, Y., and Yamazaki, M. (2004) Shape changes and vesicle fission of giant unilamellar vesicles of liquid-ordered phase membrane induced by lysophosphatidylcholine. *Langmuir* **20,** 9526–9534

75. Akiyama, T., Takagi, S., Sankawa, U., Inari, S., and Saitô, H. (1980) Saponin-cholesterol interaction in the multibilayers of egg-yolk lecithin as studied by deuterium nuclear magnetic resonance– digitonin and its analogs. *Biochemistry* **19,** 1904–1911

76. Li, X. X., Davis, B., Haridas, V., Gutterman, J. U., and Colombini, M. (2005) Proapoptotic triterpene electrophiles (avicins) form channels in membranes: cholesterol dependence. *Biophys. J.* **88,** 2577–2584

77. Todor, I. N., Lukyanova, N. Y., and Chekhun, V. F. (2012) The lipid content of cisplatin- and doxorubicin-resistant MCF-7 human breast cancer cells. *Exp. Oncol.* **34,** 97–100

78. Gayet, L., Dayan, G., Barakat, S., Labialle, S., Michaud, M., Cogne, S., Mazane, A., Coleman, A. W., Rigal, D., and Baggetto, L. G. (2005) Control of P-glycoprotein activity by membrane cholesterol amounts and their relation to multidrug resistance in human CEM leukemia cells. *Biochemistry* **44,** 4499–4509

79. Pálffy, R., Gardlík, R., Behuliak, M., Kadasi, L., Turna, J., and Celec, P. (2009) On the physiology and pathophysiology of antimicrobial peptides. *Mol. Med.* **15,** 51–59

References This article cites 78 articles, 9 of which you can access for free at:
http://www.jbc.org/content/288/20/14000#BIBL